UNIVERSIDADE NOVA DE LISBOA

FACULDADE DE CIÊNCIAS E TECNOLOGIA

DEPARTAMENTO DE QUÍMICA

JORGE MAIÃO PERES TEIXEIRA DIAS

NOBLE METAL NANOPARTICLES – Au AND Ag – FOR BIODETECTION

Dissertation submitted for obtainment of the Master's Degree in Biotechnology, by the Universidade Nova de Lisboa, Faculdade de Ciências e Tecnologia

Supervisor:

Prof. Doutor Pedro Viana Baptista (FCT/UNL)

Co-supervisor:

Prof. Doutor Ricardo Franco (FCT/UNL)

CAPARICA

2009

nº de arquivo

“Copyright”

UNIVERSIDADE NOVA DE LISBOA

FACULDADE DE CIÊNCIAS E TECNOLOGIA

DEPARTAMENTO DE QUÍMICA

JORGE MAIÃO PERES TEIXEIRA DIAS

NOBLE METAL NANOPARTICLES – Au AND Ag – FOR BIODETECTION

Dissertation submitted for obtainment of the Master's Degree in Biotechnology, by the Universidade Nova de Lisboa, Faculdade de Ciências e Tecnologia

Supervisor:

Prof. Doutor Pedro Viana Baptista (FCT/UNL)

Co-supervisor:

Prof. Doutor Ricardo Franco (FCT/UNL)

CAPARICA

2009

Acknowledgments

Thinking that a simple thank you would to the trick, I left this chapter for last. Instead it is turning out to be the hardest chapter to be written.

I would like to thank my supervisors Professor Pedro Baptista and Professor Ricardo Franco for their expertise, inspiration and more importantly, for their patience along this thesis.

For showing me the alchemy side of inorganic synthesis and for the patience to bear with me throughout my $2.3x10^8$ attempts to synthesize nanoparticles, thank you Professor Ricardo.

For the opportunity to make real science, to experience how it feels when things just do not work, to know and work with a spectacular group of people, for showing me that it is possible to have fun and still get the work done and most of all, for the trust in my capabilities that helped me achieve more than I ever thought I could, my sincere thank you, Professor Pedro. Late night science guys cannot forget you, André, Gonçalo, and João. A special gratitude is due to Gonçalo for all the guidance (you are the greatest!).

For all the friends that helped and bear with me this long year and to Catarina, for all the love and inspiration, a special thank you.

My final words have to go to my family. I thank my brother and my nephew (sorry for absent uncle…). I dedicate my thesis to my mother and sister, for putting up with me, for never forgetting that I too lived with them, despite of the 24 hours per day that I spent in the lab, and most of all, for all the love, support and comprehension.

Resumo

Devido ao seu tamanho, forma e composição, as nanopartículas metálicas possuem propriedades ópticas, químicas e magnéticas únicas. Aproveitando estas propriedades, novos biossensores têm sido desenvolvidos utilizando, principalmente, nanopartículas de ouro. As nanopartículas de prata, devido a um coeficiente de extinção da plasmónica de ressonância mais elevado, são uma alternativa para uso como marcadores em biodetecção. No entanto, contrariamente às nanopartículas de ouro, para a derivatização com oligonucleotídeos tiolados das nanopartículas de prata é necessário recorrer a protocolos morosos e complexos. Uma forma de contornar esta limitação é a utilização de nanopartículas mistas ouro-prata na forma de liga, permitindo aproveitar a fácil derivatização das nanopartículas de ouro e o maior coeficiente de extinção da plasmónica de ressonância das partículas de prata.

Este trabalho descreve a síntese e caracterização de nanopartículas mistas ouro-prata na forma de liga (50% ouro, 50% prata), e a sua derivatização com oligonucleotídeos tiolados (nanossondas) para aplicação em diagnóstico molecular. Estas novas nanossondas foram usadas para a detecção de uma sequência específica derivada do gene da subunidade β da RNA polimerase de *Mycobacterium tuberculosis*, o agente etiológico da tuberculose humana. Alvos complementares foram detectados utilizando um sistema *non-cross-linking* que consiste na comparação espectroscópica de soluções antes e depois da indução de agregação da nanossonda através do recurso à variação de força iónica. Esta nova abordagem poderá permitir, futuramente, o uso de nanopartículas mistas ouro-prata na forma de liga com outras fracções molares de ouro, ou mesmo com nanopartículas bimetálicas compostas por outros metais (por ex. Cu, Pt), para o desenvolvimento de biossensores. A conjugação destas novas nanossondas com já amplamente caracterizado sistema baseado em nanopartículas de ouro pode dar azo ao desenvolvimento de novos métodos para biodetecção específica de DNA, RNA e/ou outras moléculas.

Abstract

Metal nanoparticles possess unique optical, chemical and magnetic properties due to their size, shape and composition. Taking advantage of these properties, new biosensors have been developed using, mainly, gold nanoparticles. Silver nanoparticles, due to its enhanced surface plasmon resonance extinction coefficient are alternate candidates as labels to biodetection. However, unlike gold nanoparticles, silver nanoparticle derivatization with thiol-modified oligonucleotides requires cumbersome and time-consuming protocols. To circumvent this limitation, an approach is the use of gold-silver alloy nanoparticles, taking advantage of the ease of derivatization of gold nanoparticles and the enhanced surface plasmon resonance extinction coefficient of silver nanoparticles.

This work describes the synthesis and characterization of gold-silver alloy nanoparticles (50% gold, 50% silver) and their thiol-ssDNA functionalized counterparts (nanoprobes) for application in molecular diagnostics. These new nanoprobes were used to specifically detect a sequence derived from the RNA polymerase β-subunit gene of *Mycobacterium tuberculosis*, the etiologic agent of human tuberculosis. Complementary targets were detected using a non-cross-linking assay that consists on the spectrophotometric comparison between solutions before and after salt-induced nanoprobe aggregation. This new approach should allow the use of gold-silver alloy nanoparticles with different gold molar fractions, or even bimetallic nanoparticles composed of other metals (e.g., Cu, Pt) in the development of biosensors. The conjugation of these new nanoprobes with the well-established gold nanoparticle system can be the basis of new multiplex methods for specific DNA, RNA and/or other molecules biodetection.

List of abbreviations

Ag-nanoprobes	Thiol-ssDNA modified silver nanoparticles
AgNPs	Silver nanoparticles
AuAg-alloy-nanoprobes	Thio-ssDNA modified gold-silver nanoparticles
AuAg-coreshell-NPs	Gold-silver core-shell nanoparticles
AuAgNPs	Gold-silver alloy nanoparticles
Au-nanoprobe	Thiol-ssDNA modified gold nanoparticles
AuNPs	Gold nanoparticles
Bp	Base pairs
DLS	Dynamic Light Scattering
DNA	Deoxyribonucleic acid
ICP	Inductively Coupled Plasma
LB	Luria-Bertani; Broth
MTB	*Mycobacterium tuberculosis*
NPs	Metal nanoparticles
OD	Ultraviolet optical density
SPR	Surface plasmon resonance
ssDNA	Single-stranded deoxyribonucleic acid
TEM	Transmission Electron Microscopy

Index

List of Figures

List of Tables

1. Introduction

1.1. Nanobiotechnology

The combination of nanoscience and biotechnology originated a growing field of research - nanobiotechnology. Still in its early stages of development, it is often considered one of the key technologies of the 21st century, with areas of research that are still being defined. Currently, nanobiotechnology focus on the utilization of biological systems, such as cells, cellular components, nucleic acids and proteins, combined with organic and inorganic materials for the attainment of functional nanostructured constructs [1].

Research on biomolecular characterization has grown exponentially due to the availability of new analytical tools based on nanotechnology. For example, near-field optics, with its unprecedented resolutions, has enabled the study of biochemical processes as well as nanoscale structures of living cells [2]. Another example is the generation of devices capable of probing the cell machinery, revealing molecular-level life processes, namely, nanocarriers designed with specific antibodies for the recognition of target species and spectroscopic labels allowing new ways of diagnostic and therapeutic operations [3]; and optical nanosensors that allow the detection of individual biochemical species in subcellular locations in living cells [4]. The effect of cancer drugs in cells has been investigated using biomedical nanosensors [5], showing the future role of these new techniques in medicine.

The dynamic information of signaling processes is fundamental for the understanding of the cellular processes. Traditional techniques include an incubation of cells with fluorescent dyes in order to examine the interaction of these dyes with several compounds [6]. This interaction is not always as specific as one would desire and the dye can be transported to non-relevant intracellular sites. Another drawback is the direct relation between the dye concentration and the fluorescence signals being affected by the interaction between the dye and the chemical of interest. The use of optical nanosensors circumvents the technical issues of traditional methods as with the excitation light can be delivered to specific locations inside cells allowing a greater specificity [1,3]. These new nanoprobes have the capability of detecting important biological molecules *in vivo* at ultratrace concentrations

with the advantage, due to the very small size of the nanoprobe, of doing so in a noninvasive or minimally invasive manner [3].

1.1.1. Nanodiagnostics

Molecular recognition is fundamental for the development of clinical diagnostic tools and therapeutic modalities. Various organic molecules, possessing unique properties, have been used to achieve the recognition of different targets [7].

The intense research on nanomaterials and their properties has provided the capability to develop novel molecular recognition tools. The possibility of combining the ease of handling DNA base modification with the different modification strategies of nanomaterials as showed its applicability in spectroscopy, electrochemistry, magnetism (imaging, purification and detection) and others [8]. The incorporation of nanomaterials in these conjugates (e.g. gold nanoparticles) facilitates signal transduction, as the signal of recognition can be amplified by several orders of magnitude, make recognition more effective. They can be modified according to the function of the designed DNA probe and make application of functional DNA more practical for molecular recognition in medical diagnostics by taking advantage of the unusual interactions between nanomaterials and living systems [9]. This increase in sensitivity and flexibility presents numerous advantages over more traditional procedures, i.e. fluorescence and chemiluminescence technology [10].

Gold nanoparticles (AuNPs) in particular and their application in nanodiagnostics have received a lot of attention from the scientific community [10]. The first report of the DNA hybridization event with thiol-ssDNA modified gold nanoparticles (Au-nanoprobes) was made by Storhoff and co-workers [11], and, since then, several new approaches and applications have been reported (see Section 1.1.2. for further information).

1.1.2. Metal nanoparticles

Metal nanoparticles (NPs) possess unique optical, electronic, chemical and magnetic properties different from bulk materials of the same kind. These properties depend mainly of the size, shape and composition of the nanoparticle [12].

Noble metal NPs exhibit a strong plasmon resonance band in the visible region. This characteristic has been used in the development of biosensors for use in colorimetric detection of analytes [13,14,15,16,17,18,19].

The light absorption by NPs is related to the incident light interaction with the surface of the nanoparticle. When light of a specific energy interacts with the surface of noble metal NP, an intense localized field is induced. The coupling of the NPs conduction band electrons with the electric field of incident light, at a resonant frequency, generates a localized plasmonic oscillation on the surface of the NPs, designated by surface plasmon resonance (SPR) or LSPR, from Localized SPR [20]. Polarization of the opposite direction in the surrounding medium is consequently induced, thus reducing the restoring force for the electrons, shifting the SPR to a lower frequency. It is then possible to control the SPR wavelength by controlling the dielectric constant of the surrounding medium. The limitation of the electrons to dimensions smaller than the incident light wavelength is also a factor that contributes to the properties of these oscillations [21,22,23].

Several types of NPs of different composition, shapes and sizes can be easily obtained through chemical [24,25,26], photochemical [27] and biological [28] synthesis. Among these approaches, the most commonly used for noble metal nanoparticles has been the chemical reduction of the correspondent salt form with sodium citrate, commonly known as the "Turkevich method" [26].

1.1.2.1. Gold nanoparticles

AuNPs have been the focus of intense research due to the wide variety of molecules that can be used for their stabilization, taking advantage of the well-known chemistry involving thiol adsorption to gold [29].

In solution, monodisperse AuNPs appear red and exhibit a relatively narrow surface plasmon absorption band centered around 520 nm in the UV-Visible spectrum. In contrast, a solution containing aggregated gold nanoparticles appears blue, corresponding to a characteristic red shift in the SPR to higher wavelength. This characteristic can be related to the size and shape of the nanoparticle, refractive index of the surrounding media and inter-particle distance and can be used in colorimetric detection of analytes [10]. The AuNPs obtained by citrate-

reduction present in solution a negative charge impaired by that anion. As charged particles, they are sensitive to changes in solution dielectrics, so with the addition of NaCl the surface charge is shielded leading to a decrease in inter-particle distance and particle aggregation [1].

Reports of the use of AuNPs in immunoassays [30], DNA detection [10], detection and control of microorganisms [31] and targeted delivery of drug [32], can be found in literature.

1.1.2.1.1. DNA-functionalized gold nanoparticles

The direct functionalization of the AuNPs surface with thiol-ssDNA, generating Au-nanoprobes that recognize DNA targets of interest, can be used in highly sensitive and selective DNA detection assays. The probe strand is designed to be complementary to a target of interest and is attached to the AuNPs through chemisorption of the thiol group onto the surface of the AuNPs [33]. The method is based on color change induced by distance dependent surface plasmon absorption of AuNPs [8].

In 1996, Storhoff and co-workers reported the use of Au-nanoprobes for the colorimetric detection of DNA targets based on a cross-linking mechanism. Here, two species of probes are designed in order to each be functionalized with a DNA oligonucleotide complementary to one half of a target oligonucleotide. Thus, upon the addition of target DNA, a polymeric network of Au-nanoprobes is formed, turning the solution from red to blue [11]. Due to the extremely high molar absorptivity of AuNPs, 1000 times higher than that of organic dyes, the DNA biodetection AuNPs-based have high sensitivity, when compared to that of conventional biodetection assays using fluorescence [34].

Following a parallel approach, in 2005 Franco and co-workers reported the colorimetric detection of specific DNA detection based on a non-cross-linking mechanism. Here, Au-nanoprobe aggregation is induced by an increasing salt concentration, the presence of a complementary target preventing aggregation and the solution remains red; non-complementary or mismatched targets do not prevent Au-nanoprobe aggregation and the solution changes color from red to blue [35,36,37].

The use of Au-nanoprobe for specific DNA detection has proven its specificity and sensitivity with reports of single nucleotide polymorphism identification [37], specific mRNA detection in

as little as 0.3 µg of unamplified total RNA [35], 0.5 µg of unamplified total human RNA [38] and specific sequences of unamplified genomic DNA [33].

1.1.2.2. Silver nanoparticles

Silver nanoparticles (AgNPs) have similar properties to their gold counterparts but exhibit a higher efficiency of plasmon excitation [39], as they interact more efficiently with visible light. This interaction is a consequence of the large density of conducting electrons, their size confinement to dimensions smaller than the mean free path, and the unique frequency dependence of the real and imaginary parts of the dielectric function in the metal [40].

Like for their gold counterparts, AgNPs can be synthesized by a variety of methods depending on the nature of the nanoparticle application. The chemical reduction has the drawback of only being able to produce stable nanoparticles with <10 nm in diameter [23]. These AgNPs are not as efficient with light interaction as larger ones, doing it strictly through energy absorption. Nevertheless, they are suitable for catalysis as the main emphasis is on surface-to-volume ratio. On the other hand, the methods that allow the synthesis of larger AgNPs have the disadvantage producing a wide size distribution, lack of particle crystallinity and are costly and of difficult scale-up. However, the plasmon resonances in larger AgNPs have a significant light-scattering component that can be advantageously used in applications that require efficient optical labels, such as in chemical assays [23].

AgNPs functionalized with thiolated ssDNA (Ag-nanoprobes) have shown high sensitivity in specific DNA detection [41]. However, both AgNPs and Ag-nanoprobe are poorly stable and have lengthy, cumbersome synthesis methods, being those the probable reasons why few reports of their application in DNA detection can be found in the literature [41,42,43,44].

1.1.2.3. Bimetallic nanoparticles

Bimetallic nanoparticles are being thoroughly studied for the unique advantages that they offer over their single-metal counterparts, for example, in enhanced catalytic activity and selectivity [45,46,47], fine tuning of optical properties [22,48], magnetism [49], gene delivery [50], and electronic materials [51].

Within a single nanoparticle, the optical, electronic and magnetic properties of the bimetallic particles represent an advantageous combination of the properties of both metals. The specific properties depend however, on the arrangement of the metals within the particle, i.e., alloy or core-shell structure [3].

Bimetallic nanoparticles can be prepared via the simultaneous or the successive reduction of two metal ions, through a suitable capping or template stabilization strategy, combating steric hindrance and static-electronic repulsive force. The former is used for the production of homogeneous alloy structures [48] whereas the latter yields core-shell structured nanoparticles [52].

Gold-silver is the most interesting bimetallic system because both metals are miscible in the bulk phase [3]. It has been shown that gold-silver alloy nanoparticles (AuAgNPs) and gold-silver core-shell nanoparticles (AuAg-coreshell-NPs) blue shift with decreasing size and increasing silver content [48,53]. It has also been observed that for this system, for a constant composition, each type of nanostructure - alloy or core-shell - can be distinguished and identified solely by its optical absorbance features [53]. Thus, controlling the nanoparticles size, composition and nanostructure one can create a unique absorbance signature that can be useful in applications where nanoparticles serve as chemical labels or taggants.

So far few reports exist on the use of the gold-silver system in biomolecule detection. Cao and coworkers have reported the use of AuAg-coreshell-NPs, taking advantage of the ease of derivatization of AuNPs and the enhanced SPR extinction coefficient of AgNPs, allowing the application of the common strategies used in Au-nanoprobes assembly [54,55,56]. However, due to the thermally activated process of gold and silver atoms diffusion forming alloy nanoparticles [57], strategies are being developed to optimize their synthesis [52,54], with the disadvantage of adding complexity to an already more complex synthesis, when compared to the gold [26] and silver [58] citrate reduction method.

So far, AuAgNPs have mainly been studied because of their catalytic properties [59], as reports of the application of these NPs in biomolecule detection are inexistent.

This work describes the synthesis of AuAgNPs and their functionalization with thiol-ssDNA to generate AuAg-alloy-nanoprobes. The adaptation of these novel nanoprobes to the non-cross-linking detection method previously developed for gold nanoparticles is discussed.

1.2. Tuberculosis - etiology, relevance and nanodiagnostics

Tuberculosis (TB) is the leading cause of death from a bacterial infectious disease affecting 1.8 billion people/year. *Mycobacterium tuberculosis* (MTB) is the human etiologic agent of tuberculosis and is the best-known member of the *Mycobacterium tuberculosis* complex, a small closely related group of organisms of the genus *Mycobacterium* [60].

TB diagnosis requires lengthy and expensive methods. Nowadays MTB detection resorts mainly to three methods: (i) the Ziehl-Neelsen method which can take up to 6 weeks to develop; (ii) the BACTEC system in which MTB growth can be detected in 16 days; and (iii) the Mantoux test in which results can be obtained within 72 hours [60]. Nucleic acid amplification methods (e.g. the enhanced AMPLIFIED MTD® from Gen-Probe and the COBAS® TaqMan® MTB Test from Roche) have been developed allowing the detection of mycobacterial DNA or RNA before culture results are available [61]. Nevertheless, new and even faster detection methods are being developed, namely through gold nanoparticles based biosensors [62].

In the present work, AuAgNPs were used for the synthesis of AuAg-alloy-nanoprobes with the objective of specifically detecting a sequence derived from the RNA polymerase β-subunit gene of MTB [62].

This specific target was chosen as proof of concept of these new nanoprobes, for two main reasons:

i) It is crucial the development of faster methods for the detection of a disease that is responsible for more than 2 million deaths annually [62].
ii) The target under study has already been successfully used for the development of an Au-nanoprobe-based detection method [63], allowing the effective comparison of the system under development.

2. Materials and methods

2.1. Reagents

2.1.1. Chemical reagents

Chloroauric acid trihydrate ($HAuCl_4.3H_2O$)

Sodium citrate tribasic dihydrate 99% ($Na_3C_6H_5O_7.2H_2O$) p.a.

Phenol p.a.

Cloroform p.a.

Silver nitrate p.a.

Sodium chloride p.a.

Magnesium chloride hexahydrate p.a.

Sodium dodecyl sulfate (SDS) 90% (w/v) p.a.

Dithiothreitol ($C_4H_{10}O_2S_2$) 1 M

Sodium hidroxide (NaOH) p.a.

All the reagents used were purchased from Sigma-Aldrich and were of the highest available purity.

2.1.2. Biological reagents

Taq polimerase

GelRed®

Agarose electrophoresis grade

DNA ladder GeneRuler™

All the biological reagents used were purchased from Fermentas.

2.2. DNA oligonucleotides

Designation	5'-3' sequence	Modifications
MycoComplex1 (probe)	GGA CGT GGA GGC GAT C	5' thiol
MycoPOS (complementary DNA)	GGC CGC TGC GGC GGG GCT CAG ATC GCC TCC ACG TCC	-
MycoNEG (non-complementary DNA)	TGG ATT TAA GCA GAG TTC AAA TCT GTA CTG CAC CCT GGA G	-
pJET1fw (primer)	GCC TGA ACA CCA TAT CCA TCC	-
pJET1rev (primer)	GCA GCT GAG AAT ATT GTA GGA GAT C	-
Betaglob36 (primer)	ACT CCC AGG AGC AGG GAG GGC AGG	-
103 (primer)	CAG ATC CCC AAA GGA CTC AAA GAA CCT CTG	-

2.3. Buffers

0.1 M phosphate buffer, pH 8	0.094 M K_2HPO_4 0.006 M KH_2PO_4
0.1 M phosphate buffer, pH 7	0.0615 M K_2HPO_4 0.0385 M KH_2PO_4
0.1 M phosphate buffer, pH 8, 0.1 M NaCl	0.1 M phosphate buffer, pH 8 4 M NaCl
0.1 M phosphate buffer, pH 8, 2% SDS	0.1 M phosphate buffer, pH 8 10% SDS
TE (pH 8)	0.01 M Tris.HCl (pH 8) 0.001 M EDTA (pH 8)
AL1	0.05 M glucose 0.01 M EDTA 0.025 M Tris-HCl (pH 8)
AL2	1% SDS 0.4 M NaOH

AL3	5 M K^+ (pH 4.8) 3 M Ac^-

2.4. Instrumentation

UVmini-1240 spectrophotometer Shimadzu, Japan;

Varian Cary Eclipse Fluorescence Spectrophotometer, USA;

ICP-AES Horiba Jobin-Yvon Modelo Ultima, France;

Malvern Zetasizer Nano ZS, England;

Hitachi H-8100 Electron Microscope, Japan.

2.5. Methods

All glassware was previously treated with *aqua regia* ($HCl:HNO_3$, 1:3) and washed with milliQ ultrapure water (18.2 MΩ.cm at 25 °C).

2.5.1. Gold nanoparticles synthesis according to the Turkevich method

This method allows the synthesis of spherical gold nanoparticles.

1. Reflux a solution with a final volume of 250 mL of milliQ ultrapure water (18.2 MΩ.cm a 25 °C) containing $2.5x10^{-4}$ mol of $HAuCl_4$.
2. Add 50 mL of 38.8 mM sodium citrate to the boiling solution, and continue reflux for an additional 30 min.
3. Cool the solution to room temperature, and store in glass container at room temperature, protected from light.

Gold nanoparticle concentration was determined by the Lambert–Beer law assuming a calculated molar absorptivity for the plasmon resonance band maximum (526 nm) of $2.33\times10^8\ M^{-1}cm^{-1}$ [35].

2.5.2. Alloy Gold-Silver nanoparticles synthesis:

2.5.2.1. Link, Wang and El-Sayed method

This method allows the synthesis of alloy gold-silver nanoparticles with a gold molar ratio of 0.5.

1. Reflux a solution with a final volume of 95 mL of milliQ ultrapure water (18.2 MΩ.cm a 25 °C) containing $1.27x10^{-5}$ mol of Au and $1.27x10^{-5}$ mol of Ag.
2. Add 5 mL of 1% sodium citrate to the boiling solution.
3. Reflux the solution for an additional 30 min.
4. Cool the solution to room temperature.
5. Store in glass container at room temperature protected from light.

2.5.2.2. Alloy Gold-Silver nanoparticles suitable for functionalization with thiol-ssDNA [Dias *et al* – in preparation]

1. Reflux a solution with a final volume of 250 mL of milliQ ultrapure water (18.2 MΩ.cm a 25 °C) containing $6.35x10^{-5}$ mol of Au and $6.35x10^{-5}$ mol of Ag.
2. Add 25 mL of 1% sodium citrate to the boiling solution.
3. Reflux the solution for an additional 30 min.
4. Cool the solution to room temperature.
5. Centrifuge at 233 g for 20 minutes.
6. Filter through a 0.2 µm nylon filter (Whatman, GE Healthcare, UK).
7. Store in glass container at room temperature, protected from light.

2.5.3. Inductively Coupled Plasma (ICP), Dynamic Light Scattering (DLS) and Transmission Electron Microscopy (TEM) measurements

2.5.3.1. Inductively Coupled Plasma (ICP)

The gold and silver molar fractions of the AuAgNPs were determined by Inductively Coupled Plasma Atomic Emission Spectrometer, model Ultima (Horiba Jobin Yvon, Longjumeau, France) equipped with an RF generator of 40.68 MHz, a Czerny-Turner type monochromator

with 1.00 m (sequential), an AS500 autosampler and data acquisition software. The measured samples were diluted 1:2 in *aqua regia*.

ICP measurements were made at CQFB, FCT-UNL, Caparica, Portugal.

2.5.3.2. Dynamic Light Scattering

The hydrodynamic diameter of the citrate capped AuAgNPs was determined by Dynamic Light Scattering (DLS) using the Zetasizer Nano ZS system. A 4 mWHe-Ne laser (633 nm) was used with a fixed 173◦ scattering angle. A total volume of 500 µL of 14 ρM AuAgNP was first stabilized for 15 min at 25 ^{o}C and then measured in automatic mode. DLS measurements were made at ITQB-UNL, Oeiras, Portugal.

2.5.3.3. Transmission Electron Microscopy

The AuAgNPs morphology and diameter were determined by Transmission Electron Microscopy (TEM). Samples for TEM analysis were prepared by depositing 10 µL of the as-prepared colloidal suspensions in carbon copper grids, washing twice with 10 µL of Milli-Q water, and air dried. TEM was performed with a HITACHI H-8100 microscope operated at 200 kV. Histograms of the NP size distribution were generated in Excel; and are based on the counting of approximately 100 AuAgNPs. TEM measurements were made at ICEMS, IST, Portugal.

2.5.4. Metal nanoparticles functionalization

The nanoprobes, i.e. thiol-ssDNA functionalized nanoparticles, were synthesized according to a modification of the method described by Hurst *et al* [63].

1. Resuspend the thiol modified oligonucleotide in 0.1 M DTT followed by three extractions with ethyl acetate, followed by purification with a NAP-5 column (GE HealthCare, United Kingdom) according to the manufacturer's instructions.
2. Add the purified oligonucleotides to the nanoparticles accordingly to the desired oligonucleotide/NPs ratio. Bring the solution to 0.01 M phosphate buffer pH 8 and 0.01% SDS.

3. Allow the oligonucleotide/gold nanoparticle solution to incubate at room temperature for 20 min.
4. Increase NaCl concentration to 0.05 M using 0.01 M phosphate buffer 1.5 M NaCl 0.01% SDS pH 8, followed by 20 min incubation at room temperature. This process is repeated once with an increment of 0.05 M NaCl, and thereafter for every 0.1 M NaCl increment until a concentration of 0.3 M NaCl is reached.
5. Incubate at room temperature for 16 hours.
6. To remove excess oligonucleotides, centrifuge the solution and remove the supernatant. Resuspend the pellet in 0.01 M phosphate buffer 0.1 M NaCl pH 8. Repeat this washing process 5 times.
7. Store at 4 ^{o}C protected from light.

2.5.5. Plasmid DNA isolation

1. Inoculate 10 ml of LB broth supplemented with ampicillin from either a single colony or a glycerol stock derived from a single colony. Grow the culture overnight (14 hours) at 37 ^{o}C with shaking at 200 rpm.
2. Transfer the cells to 1.5 mL eppendorf tubes and centrifuge at 9500 rpm in a benchtop microfuge. Remove the media and replace it with 150 µl of solution AL1.
3. Gently resuspend the cells and place them in ice.
4. Add 300 µl of AL2 and mix by gentle inversion. Incubate the tube on ice for 5 minutes.
5. Add 225 µl of Al3 and mix by very gentle inversion. Leave the sample on ice from 15 minutes to 4 hours.
6. Centrifuge the sample at 13000 rpm for at least 15 minutes.
7. Remove volumes of 630 µl of the resulting supernatant and place in new tubes.
8. Add 1260 µl of 100% ethanol. Leave the tubes at:

   -20 ^{o}C 2 hours or

   -70 ^{o}C 45 minutes
9. Pellet the DNA at 13000 rpm for 10 minutes, wash with 70% ethanol and dry.
10. Resuspend in 200 µl of H_2O. Pool together the content of (n) tubes, if suitable.

11. Add RNAse (1:50 total volume), allow to digest for at least 3 hours at 37 ^{o}C.
12. Add an equal volume of phenol and mix by vortexing for 1 minute.
13. Centrifuge the sample at 13000 rpm for 3 minutes. Remove 450 µl of the aqueous phase and add an equal volume of chloroform/isoamyl alcohol (24:1), mix by vortexing for 1 minute.
14. Centrifuge again at 13000 rpm for 3 minutes. Remove 400 µl of the aqueous phase and place in a new tube.
15. Add 1:10 volume of 3 M $NaCH_3COO$ pH 7.5 and two volumes of 100% ethanol to the sample to precipitate the DNA as indicated in step 8.
16. Pellet the DNA at 13000 rpm for 10 minutes, wash with 70% ethanol, dry and resuspend in 40 µl of H_2O.

2.5.6. PCR amplification

The following standard premix was prepared for each 25 µL.

Table 1: PCR amplification program reaction.

Component	Final concentration
Ultrapure miliQ water autoclaved (pH 7.0)	-
PCR buffer 10x	1x
dNTPs mix (25 mM each nucleotide)	200 µM (each dNTP)
primer mix (25 pmoles/µL each primer)	0.4 µM (each primer)
Taq DNA polymerase	1 U/25 µL
Plasmid DNA template (200 ng/µL)	10 g/µL

For MycoPOS samples the amplification parameters were as follows:

Initial denaturation	95 °C	5 minutes	
Denaturation	95 °C	30 seconds	35 cycles
Primer annealing	58 °C	30 seconds	
Extension	72 °C	45 seconds	
Final extension	72 °C	7 minutes	

For MycoNEG samples the amplification parameters were as follows:

Initial denaturation	95 °C	5 minutes	
Denaturation	95 °C	30 seconds	30 cycles
Primer annealing	51 °C	30 seconds	
Extension	72 °C	45 seconds	
Final extension	72 °C	7 minutes	

2.5.7. Hybridization assays

Hybridization assays were carried out using an adaptation of the protocol previously described by Baptista *et al* [35] for specific RNA sequences detection using AuNP nanoprobes.

Prepare assay solutions containing the nanoprobes and target DNA by mixing the desired concentration of DNA with the nanoprobe at a given final concentration. After an incubation step at 95 °C for 10 min for DNA denaturation, samples are cooled to 20 °C at a 0.1 °C/seg ratio. Allow the mixtures to stand for 20 min, then add a salt solution to a predetermined final ionic strength concentration. Blank measurements are made in exactly the same conditions but replacing DNA for an equivalent volume of 10 mM phosphate buffer. After 20 min at room temperature assay the samples by UV-Visible spectroscopic measurements of the plasmon resonance.

2.5.7.1. PCR product DNA

The PCR products, with 384 bp in length, were obtained by PCR (Section 2.5.6) and purified after gel band excision. This purification is needed so as to remove the ions present in the reaction media that could hamper the nanoprobe assay. The presence of the complementary sequence to the AuAg-alloy-nanoprobes in the sample that tested positive for *M.* tuberculosis was confirmed by DNA sequencing. A sample containing an unrelated PCR product with approximately the same base pair number (400 bp) was used as negative control, and its size was confirmed by gel electrophoresis.

2.5.7.2. Plasmid DNA

Plasmid DNA, with 3350 bp in length, was obtained as described above (Section 2.5.5.). The presence of the complementary sequence to the AuAg-alloy-nanoprobes was confirmed by DNA sequencing. A sample of unrelated plasmid DNA with approximately the same base pair length (3500bp - confirmed by gel electrophoresis), was used as a negative control.

3. Results and discussion

3.1. Summary

Gold-silver alloy nanoparticles with a molar ratio of 50% Ag and 50% Au were successfully synthesized and characterized via inductively coupled plasma (ICP), dynamic light scattering (DLS) and transmission electron microscopy (TEM). These nanoparticles were subsequently functionalized with thiol-linked ssDNA to yield AuAg-nanoprobes. These novel AuAg-alloy-nanoprobes were used in a non-cross-linking based colorimetric detection of specific DNA sequences from *Mycobacterium tuberculosis*.

3.2. Gold-Silver alloy Nanoparticles

Gold-silver alloy nanoparticles can be synthesized with different ratios of each metal, where increasing molar fractions of silver lead to a typical blue-shift of the SPR peak [48]. This study focused on a ratio of 50% Ag and 50% Au, taking advantage of the alkyl thiol greater affinity for the gold [54], while containing a sufficient amount of silver to increase the NPs' extinction coefficient [39,41].

3.2.1. Link, Wang and El-Sayed method

3.2.1.1. Synthesis and characterization

AuAgNPs were synthesized according to Link *et al* [48] and characterized by ICP to analyze gold and silver molar fractions, DLS to measure the hydrodynamic diameter of the nanoparticles and TEM to measure its effective radius and determine their exact shape.

A single SPR peak can be observed for the resulting nanoparticles (Figure 1). Observation of a single SPR peak indicates that a bimetallic alloy was formed [22,65].

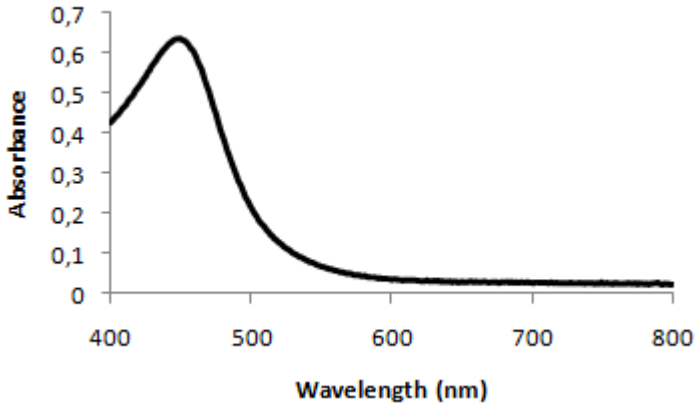

Figure 1: UV-Visible spectrum of the AuAgNPs.

ICP data revealed that the AuAgNPs have an elemental composition of 46% gold and 54% silver (see annex 6.2 for calculation of the elemental composition). DLS data indicated an average hydrodynamic NPs radius of 29.4 nm (Figure 2).

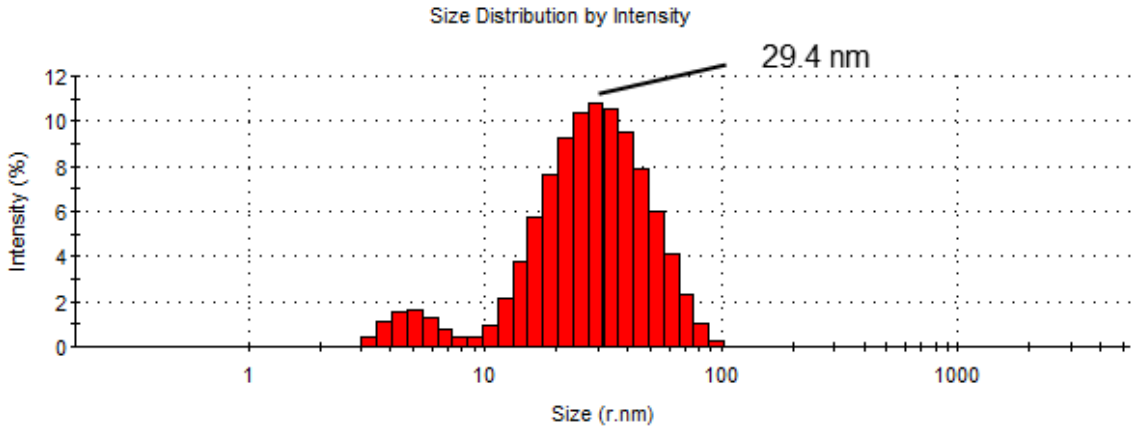

Figure 2: Size distribution (radius, nm) by intensity percentage of the AuAgNPs determined by dynamic light scattering. The average hydrodynamic NPs radius was determined to be 29.4 nm.

Figure 3A shows a TEM image of the AuAgNPs. The average radius of the nanoparticles was determined to be 12.5 nm, based on the counting of approximately 100 nanoparticles from 5 micrographs. The corresponding size histogram is presented in figure 3B. The measurements obtained by analysis of the TEM micrographs are in agreement with results by Link *et al* [48] obtained for AuAg alloy nanoparticles with the same gold molar fraction (Table 2).

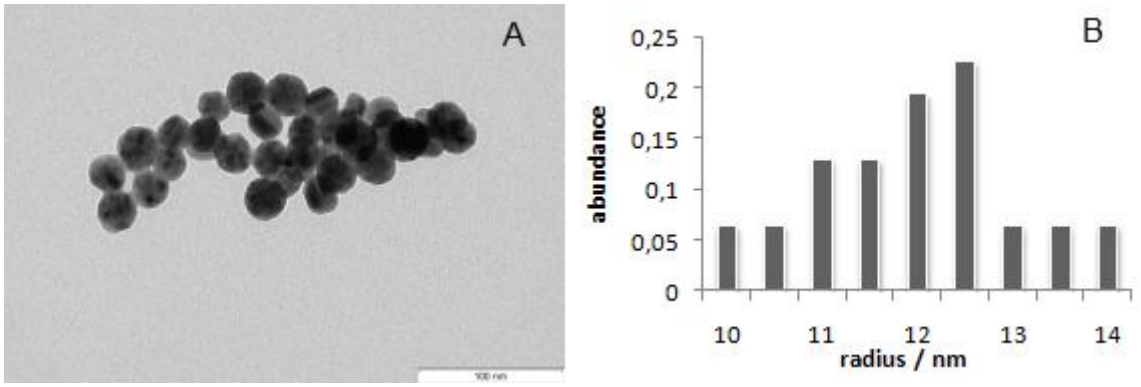

Figure 3: TEM image of the AuAgNPs (**A**). Size histogram corresponding to measurements of approximately 100 AuAgNPs from 5 micrographs (**B**). The average radius was determined to be 12.5 nm.

In order to allow a complete UV-Visible spectra analysis (e.g. calculation of the AuAgNPs concentration), the molar extinction coefficient (ε) of the involved species is required. Link *et al* [48] demonstrated that the Mie theory cannot be applied to AuAgNPs, so, ε was calculated for the synthesized NPs using the data obtained from ICP and TEM characterization (see annex 6.3. for calculation of the molar extinction coefficient). DLS measures the hydrodynamic radius of the NPs and the TEM measures the effective radius of the NPs, thus a more accurate calculation of the ε can be obtained using the latter. Therefore, the NPs radius measured by TEM was used for the calculation of the ε.

Using data of the NPs' metal composition and diameter, the number of gold and silver atoms in each nanoparticle was calculated based on known densities for the individual metals, and consequently the volume occupied by all NP could be estimated. Thus, as the final volume was known, approximate AuAgNPs concentrations could be used to plot an Absorbance vs. concentration curve that allowed the calculation of ε. The value obtained is in accordance with the referred by Link *et al* [48] for 12.5 nm radius nanoparticles with an approximate 0.5 molar gold fraction (Table 2).

Table 2: Characterization of AuAgNPs.

Characteristics	**AuAgNPs in this work**	**Link *et al* [48]**
λ_{max} (nm)	450	455
Nanoparticle radius (nm)	12.5	12.5
Hydrodynamic radius (nm)	29.4	-
Gold fraction (x_{Au})	0.46	0.54
Molar extinction coefficient ε ($M^{-1}cm^{-1}$)	$1.42x10^9$	$1.8x10^9$

Since the objective of this work was the functionalization of AuAgNPs with thiol-ssDNA, and the protocol adopted to do so described by Hurst *et al* [64] requires a buffered pH 8 medium, the AuAgNPs stability for different pH values was studied. Extensive aggregation was observed when the NPs solution came in contact with the pH electrode. Thus, using buffered solutions, the variation of the SPR peak profile induced by pH was only studied for pH 7 and pH 8. These two pH values were selected because, as referred, the functionalization protocol requires a buffered pH 8 medium and because in future hybridization assays a buffered pH 7 medium is required for suitable DNA hybridization [11]. At both pH tested the synthesized NPs maintained their characteristic SPR peak profile (see annex 6.1 figure 20).

Storhoff *et al* [15] proposed that, for gold nanoparticle-thiol-ssDNA conjugates, an increased repulsion between the particles derived from the electrostatic charges of the exposed bases of single stranded DNA, conferring to these conjugates the capacity to endure higher ionic strength than their non-functionalized counterparts. This capacity allows the assumption that the sodium citrate capping was replaced by thiol-ssDNA, being an indication of functionalization efficiency. Thus, the aggregation behavior of the AuAgNPs, with increasing NaCl concentration, was analyzed by UV-Visible spectroscopy. A 0.25 nM solution of AuAgNPs aggregated instantaneously after NaCl addition at low concentrations (0.1 M NaCl). In the non-aggregated form, the SPR peak appears at approximately 450 nm; in the aggregated form, there is a diminishing of the SPR peak intensity and shifting to the red region of the spectrum, to around 720 nm (Figure 4).

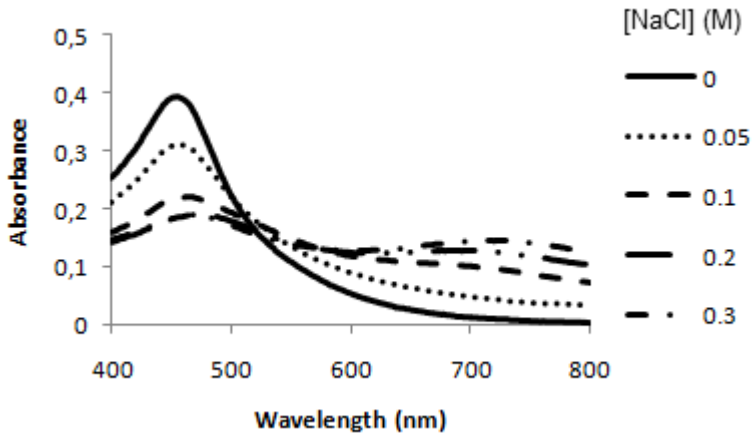

Figure 4: AuAgNPs stability against salt-induced aggregation. Visible spectra of AuAgNPs (0.25 nM) in 10 mM phosphate buffer pH 8, at room temperature, for different NaCl concentrations.

3.2.1.2. Gold-Silver alloy nanoparticles functionalization

The functionalization protocol was adapted from Hurst *et al* [64] (see Section 2.5.4) Following a similar approach of AuNPs functionalization, AuAg-alloy-nanoprobes were synthesized by derivatizing 2 ml of an aqueous AuAgNPs solution with 1 UV optical density (OD) of thiol-ssDNA with the sequence 5' - GGA CGT GGA GGC GAT C – 3', and a salting aging procedure was carried out. It was also considered the need to obtain a final AuAg-alloy-nanoprobes concentration allowing further testing and characterization.

During the ageing step, upon salt addition (0.3 M NaCl), the AuAgNPs aggregated, as shown by the decrease and red-shift of the SPR (Figure 5). This might be due to the insufficient oligonucleotide surface coverage that, once the citrate capping is removed, is not able to compensate for the increase in ionic strength [11]. These NPs were judged unsuitable for functionalization and an alternative synthesis was designed so as to attain AuAg-alloy-nanoprobes.

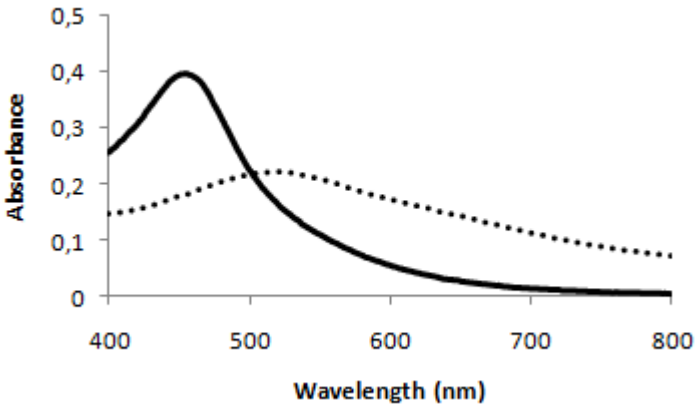

Figure 5: AuAgNPs and AuAg-alloy-nanoprobes before and after functionalization. Visible spectra of AuAgNPs before (—) and after (···) functionalization with a 1 OD / 2 mL AuAgNPs ratio.

3.2.2. *Dias* method

Based on the previous functionalization results, two hypotheses were put forward:

i) Increasing the amount of thiol-ssDNA would allow a ratio of oligonucleotide/NP for which the functionalization of these AuAgNPs is possible.

ii) Decreasing the amount of citrate in the AuAgNPs synthesis would lead to a decrease in the capping extent with concomitant increase of the nanoparticles' average diameter. The presence of less citrate molecules and more gold atoms in the surface of each nanoparticle would, in theory, allow a larger number of thiol-ssDNA at the nanoparticle surface.

In spite of the simple concentration adjustment proposed by strategy i), this would not only make the process more costly (increase in amount of oligonucleotide needed) as it would provide small volumes of AuAg-alloy nanoprobes, not sufficient for an efficient characterization and application in hybridization assays.

Thus, strategy ii) was followed. Because the used metal concentrations are too high to unsure complete solubility of Ag^+ in the presence of Cl^- from the gold salt [66], it was also decided to add a centrifugation step followed by filtration (see seection 2.5.2.2.), to avoid AgCl precipitate interference during nanoprobe synthesis.

3.2.2.1. Synthesis and characterization

This new set of AuAgNPs (now herein designated *Dias* method set) was characterized by ICP, DLS and TEM.

ICP data revealed that the AuAgNPs of the *Dias* method set have an elemental composition of 49% gold and 51% silver (see annex 6.2 for calculation of the elemental composition).

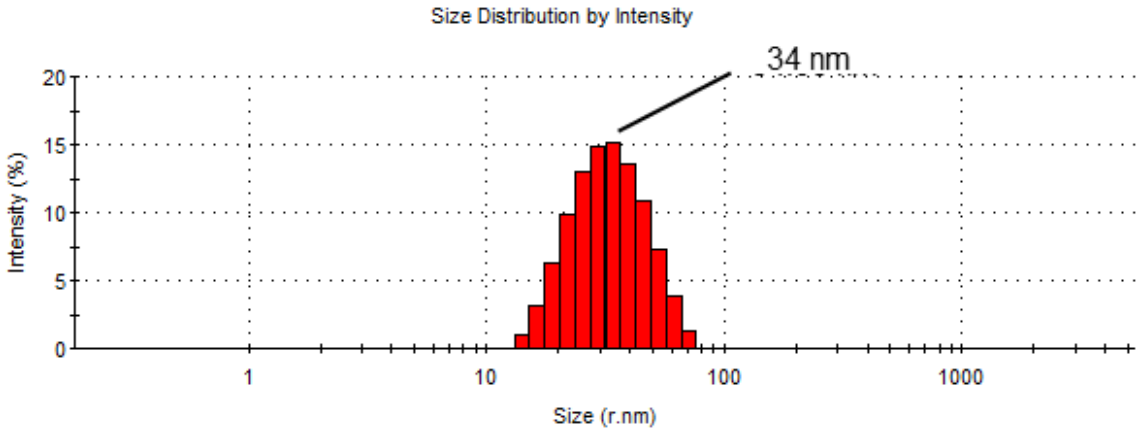

Figure 6: Size distribution (radius, nm) by intensity percentage of the *Dias* method set determined by dynamic light scattering. The average hydrodynamic NPs radius was determined to be 34 nm.

DLS data indicated an average hydrodynamic NPs radius of 34 nm (Figure 6).

Figure 7A shows a TEM image of the *Dias* method set. Based on the counting of approximately 100 nanoparticles from 5 micrographs, the average radius of the nanoparticles was determined to be 21 nm (Figure 7B).

Table 3 summarizes the characterization of both sets of AuAgNPs.

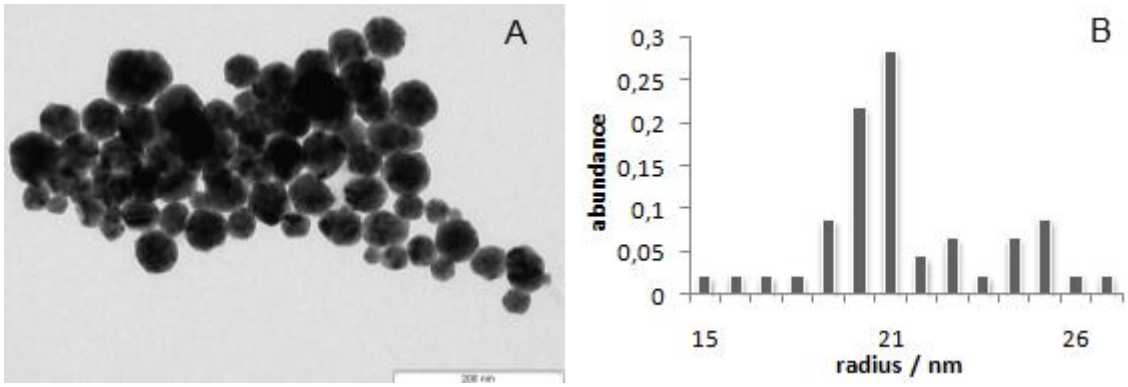

Figure 7: TEM image of the AuAgNPs (**A**). Size histogram corresponding to measurements of approximately 100 AuAgNPs from 5 micrographs (**B**). The average radius was determined to be 21 nm.

Table 3: Synthesized AuAgNPs characteristics.

AuAgNPs	**Link, Wang and El-Sayed method set**	***Dias* method set**
λ_{max} (nm)	449	451
Gold fraction (x_{Au})	0.47	0.49
Hydrodynamic radius (nm)	29.4	34
Nanoparticle radius (nm)	12.5	21
pH	-	7.5
ε ($M^{-1}cm^{-1}$)	$1.42x10^{9}$	$3.21x10^{10}$

The measurements obtained by analysis of the TEM and DLS data indicate that, possibly, the *Dias* method set presents a smaller radius of citrate capping (i.e. the difference between hydrodynamic radius and metal radius). Nevertheless, further characterization is needed to confirm these observations.

The data obtained by ICP and TEM characterization of the AuAgNPs allowed calculation of ε = $3.21x10^{10}$ $M^{-1}cm^{-1}$ (see annex 6.3. for calculation of the molar extinction coefficient). Since there are no reports of the relationship between the size and gold molar fraction and the ε value of the AuAgNPs, the calculated ε can only be compared to that of AuNPs with approximately 40 nm in diameter (ε = $6.06x10^{9}$ $M^{-1}cm^{-1}$) [67]. The verified fivefold increase of the ε for the AuAgNPs can be explained by the incorporation of silver in the AuAgNPs as already has been observed by several authors [54,55,56].

The obtained AuAgNPs spectra showed only one SPR peak indicating the formation of the desired alloy structure (Figure 8).

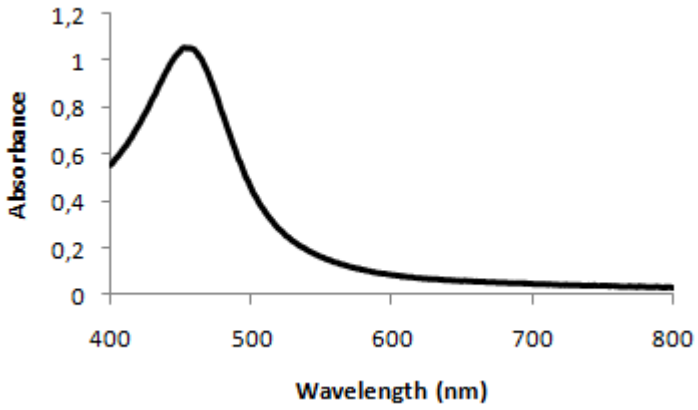

Figure 8: Visible spectrum of the AuAgNPs obtained by the *Dias* method.

The SPR peak profile variations were characterized as function of pH and increasing ionic strength of the medium. The measured pH for the AuAgNPs solution was 7.5. Here, a titration was possible as the nanoparticles did not show aggregation when in contact with the pH electrode. The AuAgNPs solution pH was changed via addition of either NaOH or HCl. The variations induced in the SPR peak profile were followed by UV-Visible spectroscopy (see annex 6.1 Figure 21).

It was observed that, for a pH range from 3.3 to 11.7, the AuAgNPs maintain their characteristic SPR peak profile. Thus, one can assume that any NPs aggregation in nanoprobe synthesis or in hybridization assays performed in this pH range will not be due to the pH of the reaction.

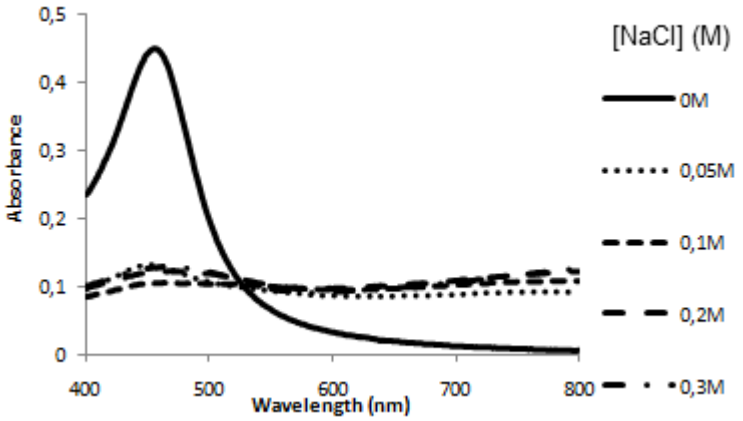

Figure 9: AuAgNPs stability against salt-induced aggregation. Visible spectra of AuAgNPs (14 ρM) in 10 mM phosphate buffer pH 8, room temperature, at different salt (NaCl) concentrations.

The ionic strength assay was performed as already described in section 3.1.1.1.

The SPR peak of the non-aggregated form maintains its characteristic profile, but the intensity of the peak diminishes upon aggregation, when increasing the ionic strength. At NaCl concentrations as low as 0.05 M instantaneous AuAgNPs aggregation occurred - Figure 9.

Considering that the AuAgNPs withstand high temperatures during the denaturation and hybridization steps (see section 2.5.7.), the stability of AuAgNPs was also assessed at those temperatures. The SPR peak profile variations of the UV-visible spectra of AuAgNPs induced by ionic strength and temperature were studied. A titration was performed with a NaCl concentration gradient, in a buffered medium, pH 7 and pH 8, for a AuAgNPs concentration of 14 ρM. This characterization was performed with and without a prior incubation step at 95 ^{o}C for 10 min, cooled to 20 ^{o}C at a 0.1 ^{o}C/seg rate and another incubation step at 20 ^{o}C for 17 min. After salt addition the samples were allowed to stand for 20 min at room temperature, followed by UV-Visible spectroscopy. All assays were carried out in triplicate.

Figure 9 shows that aggregation does not promote a clear red-shift of the SPR peak. There is a slight red-shift of the SPR peak with a concomitant broadening of its form, making difficult to determine the absorbance maximum of a well-defined peak. Hence, as described by Weisbecker *et al* [68], to facilitate interpretation of the spectroscopy data in this work, the

ratio (herein designated Abs ratio) between soluble and aggregated AuAgNPs was calculated. For Abs ratio calculation the fraction of the integrated absorbance peak between 400 nm and 550 nm, and between 550 nm and 700 nm, was used, thus providing a quantitative measure of the NP aggregation extent. Considering the calculated Abs ratio, it is possible to distinguish between the non-aggregated and the aggregated forms using a threshold of 1 (Figure 10).

Figure 10 shows that temperature promotes the diminishing of the Abs ratio at room temperature and 95 ^{o}C and at both pH tested. This indicates a significant aggregation of the AuAgNPs.

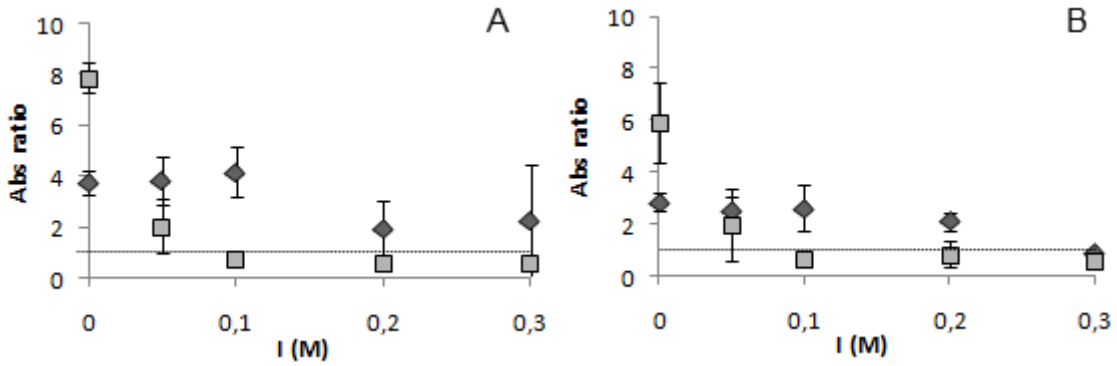

Figure 10: AuAgNPs stability against salt-induced aggregation. Absorbance ratio of AuAgNPs (14 ρM) in a 10 mM phosphate buffer pH 7 (A), or pH 8 (B), at room temperature (squares) and 95 ^{o}C (diamonds), at different ionic strength concentrations (NaCl).

It is also possible to observe that, for the assays carried out at 95 ^{o}C, the standard deviation values are higher than those of the assays at room temperature. This indicates that submitting the AuAgNPs to 95 ^{o}C before salt addition has effect on the AuAgNPs salt-induced aggregation.

Considering that in hybridization assays it is necessary to use a divalent salt ($MgCl_2$), which induces AuAg-alloy-nanoprobe aggregation at lower ionic strength concentrations, comparatively to NaCl (see section 3.2.2.), its effect in AuAgNPs was studied. The SPR peak profile variations of the UV-visible spectra of AuAgNPs induced by ionic strength and temperature were studied. The assays were carried out as already described for the NaCl study.

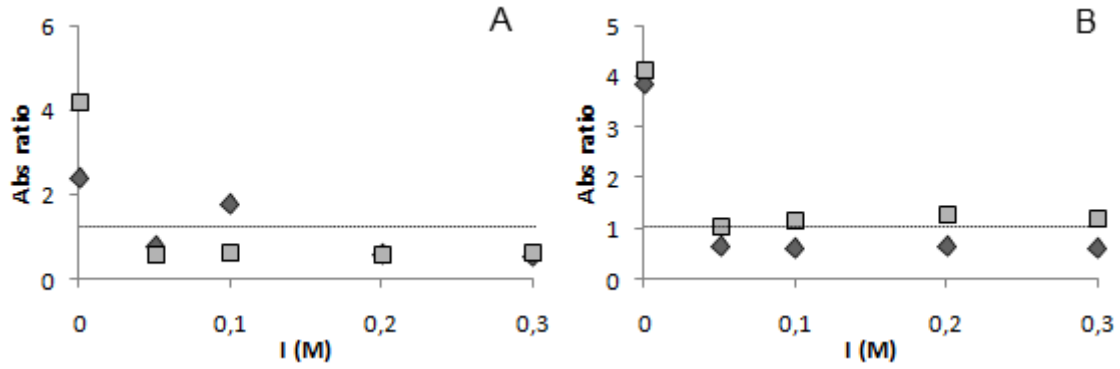

Figure 11: AuAgNPs stability against salt-induced aggregation. Absorbance ratio of AuAgNPs (14 ρM) in a 10 mM phosphate buffer pH 7 (A), or pH 8 (B), at room temperature (squares) and 95 ^{o}C (diamonds), at different ionic strength concentrations ($MgCl_2$).

When using $MgCl_2$, all samples showed extensive aggregation (Abs ratio < 1) - Figure 11. Thus, $MgCl_2$ induces AuAgNPs aggregation at lower values of ionic strength compared to NaCl. Pacey *et al* [69] reported that monovalent salts induce a greater broaden of the SPR peak in AuNPs comparatively to the divalent salts. This can be explained with the fact that an increase in ionic strength decreases the Debye length [70]. As the Debye length decreases so does the mean distance of closest approach between nanoparticles, to a point where aggregation occurs. The author showed that despite the concentration effect, the AuNPs were farther apart for divalent cations than for monovalent cations, this indicated that, more than ionic strength, it is the cation surface adsorption that induces nanoparticles' aggregation. However, this was not verified for the AuAgNPs with NaCl and $MgCl_2$. Thus, the effect of other monovalent and divalent salts should be studied, as there is no report of the effect on monovalent and divalent salts in AuAgNPs aggregation profile.

3.2.2.2. *Dias* method set functionalization

The functionalization procedure, as already described in section 3.2.1.2., was performed with these AuAgNPs.

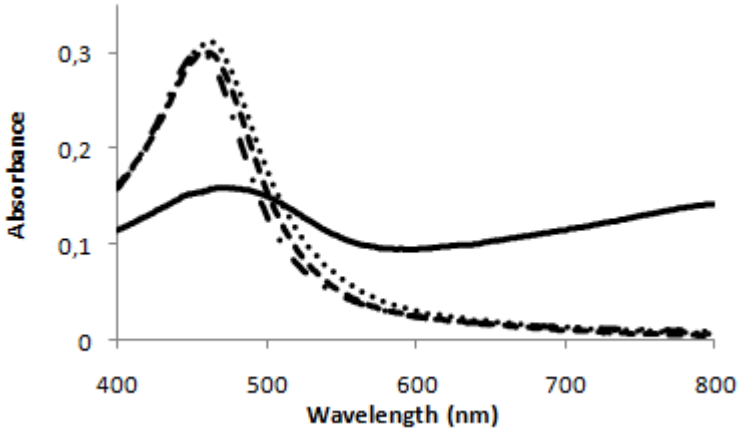

Figure 12: AuAgNPs and AuAg-alloy-nanoprobes before and after salt-induced aggregation. Visible spectra of AuAgNPs (14 ρM) (– · –) and AuAg-alloy-nanoprobes (14 ρM) (––) before and AuAg-alloy-nanoprobes (···) and AuAgNPs (—) after addition of NaCl to a final concentration of 2 M. AuAg-alloy-nanoprobes were functionalized with a 1 OD/2 mL AuAgNPs ratio.

The UV-Visible spectrum of the AuAg-alloy-nanoprobes showed that the SPR peak profile was maintained after the functionalization procedure, with a small 7 nm red-shift (Figure 12). This shift can be related to the nanoparticles surface modification, given that the functionalization procedure promotes changes in the nanoparticles diameter and surface charge distribution [22]. It is also possible to observe that at a NaCl concentration of 2 M, the AuAg-alloy-nanoprobes are in their non-aggregated form maintaining their SPR peak profile; whereas the AuAgNPs are in the aggregated form (Figure 12). This suggests that the sodium citrate capping was replaced by thiol-ssDNA, making the AuAg-alloy-nanoprobes more stable than the AuAgNPs at the tested ionic strength. This increase of stability can be related to an increased repulsion between the particles derived from the electrostatic charges of the exposed bases of single stranded DNA, as proposed by Storhoff *et al* [15] for gold nanoparticle-thiol-ssDNA conjugates.

Having successfully functionalized the AuAgNPs synthesized accordingly to the *Dias* method, all the subsequent work was performed with this AuAgNPs set.

In order to optimize the functionalization procedure other oligonucleotide OD/AuAgNPs volume ratios were tested, increasing the volume of AuAgNPs used.

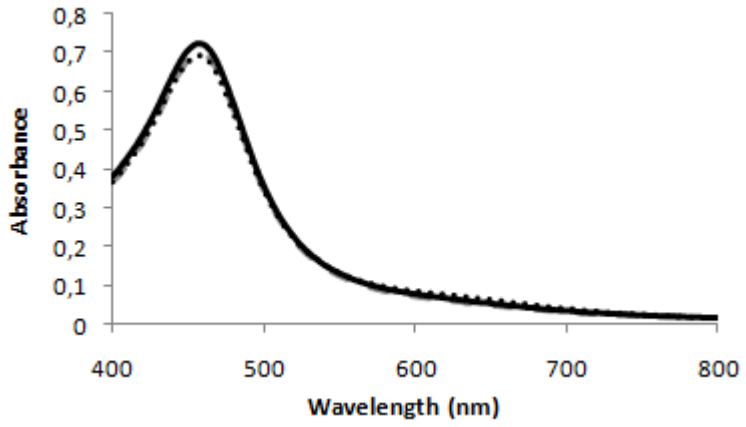

Figure 13: AuAg-alloy-nanoprobes functionalized with several oligonucleotide/AuAgNPs ratios. Visible spectra of AuAg-alloy-nanoprobes (22 ρM); ratio 1 OD/3.8 ml AuAgNPs (⋯); ratio 1 OD/2.8 ml AuAgNPs (—) and ratio 1 OD / 2 ml AuAgNPs (––).

All ratios tested yielded stable AuAg-alloy-nanoprobes (Figure 13). The functionalization procedure, for all ratios tested, had an approximate 2% yield.

The batches obtained with the 1 OD/2 ml AuAgNPs and 1 OD/2.8 ml AuAgNPs ratios maintained stability for, at least, three months after synthesis. The batch obtained with the 1 OD/3.8 ml AuAgNPs ratio aggregated during the washing process, thus no further studies were performed with this batch.

The low yield of the functionalization procedure forced the use of a low AuAg-alloy-nanoprobes concentration in hybridization assays. As it will be discussed in section 3.2.2., for the chosen AuAg-alloy-nanoprobe concentration the SPR peak intensity is very low, making it difficult to obtain a clear discrimination between the non-aggregated and the aggregated forms. Over the several functionalizations carried out, it was observed that the use of 0.01M phosphate buffer, pH 8, 0.1M NaCl led to nanoprobe adsorption to the eppendorf tubes walls. This influenced greatly the functionalization yield, as it became extremely difficult to ressuspend the nanoprobe. In an attempt optimize the washing process, the washing buffer was modified to 0.01M phosphate buffer, pH 8. This small modification resulted in an increment in the functionalization yield. A 46% yield was attained, an improvement in 23 fold compared to the 2% obtained with the initial protocol. With this modification, it became

viable to characterize the same batch of AuAg-alloy-nanoprobes to a higher final concentration.

The quantification of nanoparticle surface functionalized oligonucleotides was determined using "Quant-iT™ OliGreen® ssDNA reagent and kit" and fluorescence spectroscopy.

Table 4: Quantification of nanoparticle surface functionalized oligonucleotides.

Ratio	Yield (%)	Thiol-ssDNA per NP (ρmol/cm^2)	Thiol-ssDNA strands per NP
1 OD/ 2 ml AuAgNPs	12	303,9	9638
1 OD/ 2.8 ml AuAgNPs	31,8	590,2	19697
1 OD/ 2.5 ml AuNPs	56,7	26,7	113

Comparing AuAg-alloy-nanoprobes functionalization yields (Table 4), it is evident that with the 1 OD/2.8 ml AuAgNPs ratio one can bind more oligonucleotides per cm^2, thus making this ratio the most suitable for AuAg-alloy-nanoprobes.

To be able to compare functionalization efficiency, a gold-nanoprobe was synthesized, following the same protocol as the one used for AuAg-alloy-nanoprobes. The data obtained for the Au-nanoprobe is in concordance with the described for a 20 nm in diameter gold nanoparticle [71].

The difference between Au-nanoprobe and AuAg-alloy-nanoprobes functionalization efficiencies can be explained by the different affinity of the thiol group for silver and gold. The affinity for gold is much higher, and assuming that in AuAgNPs half of the surface is occupied by silver, there will be areas where there was little or no functionalization. The difference in efficiency can also be explained by the difference of the NPs' diameter between AuAgNPs (42 nm) and AuNPs (20 nm). Mirkin *et al* [72] recently demonstrated for AuNPs that as the nanoparticle diameter increases the surface coverage decreases. This is due to the diminishing nanoparticle curvature as function of diameter increase, causing higher repulsion between ssDNA, thus affecting functionalization yield.

In this work, a C_6 spacer between the –SH and oligonucleotide sequence is used. The purpose of this spacer is to move the recognition sequence further from the particle surface

reducing steric hindrance within this region. It has been shown that different types of spacers have different impacts in functionalization yields [63]. Therefore, different spacers should be tested in order to study their influence in AuAgNPs functionalization.

3.3. AuAg-alloy-nanoprobes characterization:

3.3.1. Effect of ionic strength and temperature

Considering that the protocol used for specific DNA detection (see section 2.5.7.) is an adaptation of the described for the Au-nanoprobes [35] it is necessary to characterize the AuAg-alloy-nanoprobes ionic strength and temperature induced SPR peak profile variations. A titration was performed both with a NaCl and a $MgCl_2$ concentration gradient in a buffered medium at pH 7 and pH 8, for a AuAg-alloy-nanoprobes concentration of 5 ρM and 14 ρM. This characterization was performed with a prior incubation step at 95 ^{o}C for 10 min, followed by a cooling step at the rate of 0.1 ^{o}C/seg and another incubation step at 20 ^{o}C for 17 min. After salt addition, the samples are allowed to stand for 20 min at room temperature. This titration was followed by UV-Visible spectroscopy.

The salt concentration that promotes AuAg-alloy-nanoprobes (5 ρM) aggregation (Abs ratio < 1; see annex 6.1 figure 22A) was 1.5 M for NaCl and 0.06 M for $MgCl_2$ at pH 7 (Table 5). At pH 8 it becomes more difficult to discriminate aggregated from non-aggregated form (see annex 6.1 figure 22B) for the tested salt concentrations. This stabilization may be due to the presence of DNA molecules. At pH 8, DNA is more negatively charged than at pH 7, promoting a higher electrostatic repulsion between DNA molecules, thus conferring a higher stability. The salt concentration required to promote aggregation at 14 ρM AuAg-alloy-nanoprobe concentration was 2 M for NaCl and 0.014 M for $MgCl_2$, for both pH tested (Table 5).

Table 5: Salt concentration required to promote AuAg-alloy-nanoprobes aggregation for both pH tested.

		pH							
		7				8			
[AuAg-alloy-nanoprobe] (ρM)	**Oligonucleotide/AuAgNPs ratio**	**[NaCl] (M)**	**I (M)**	**[$MgCl_2$] (M)**	**I (M)**	**[NaCl] (M)**	**I (M)**	**[$MgCl_2$] (M)**	**I (M)**
5	1 OD/2.8 ml AuAgNPs	1.5	1.5	-	-	-	-	-	
14	1 OD/2.8 ml AuAgNPs	2	2	0.014	0.048	2	2	0.014	0.048
	1 OD/2 ml AuAgNPs	2.5	2.5	-	-	-	-	-	-

Calculating the ionic strength concentration, given by equation (1), it can be determined that for AuAg-alloy-nanoprobe aggregation to occur using NaCl it is necessary higher values of ionic strength than when using $MgCl_2$.

(1) $I = \frac{1}{2} \sum_{i=1}^{n} c_i z_i^2$, where c_i represents the molar ion concentration and z_i the ion valence.

This indicates that, besides the variation of ionic strength, other factors must be involved in nanoprobe aggregation induced by these cations, since the counter-anion is common (Cl^-). One explanation may be based on the Mg^{2+} known capacity to interact with DNA phosphate groups [74]. Although sodium ions can also bind to DNA phosphate groups, Mg^{2+} can coordinate two phosphate groups of different DNA molecules promoting nanoprobe approximation, thus potentiating the ionic strength effect in the aggregation process.

To determine which oligonucleotide/AuAgNPs ratio allows a more efficient DNA detection hybridization assays were carried out using the protocol described in 2.5.7. The salt concentration required to promote AuAg-alloy-nanoprobe aggregation of the nanoprobe synthesized with the 1 OD/2 ml AuAgNPs ratio was previously determined (Table 5). A final 23.3 ρmol DNA concentration was used. Complementary DNA detection was carried out using a synthetic complementary DNA sequence (herein designated as MycoPOS) or a non-complementary DNA sequence (herein designated as MycoNEG). As reference (Blank), an assay where the DNA volume is replaced by buffer solution was carried out.

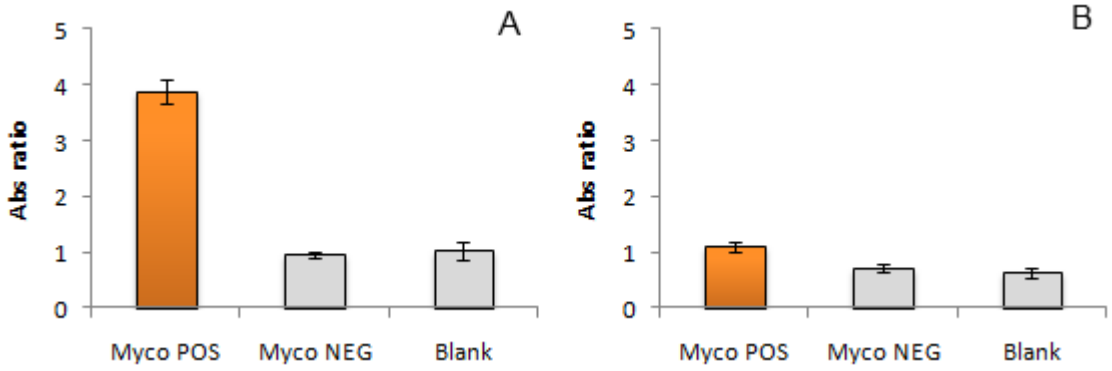

Figure 14: Detection of specific nucleic acids sequence with AuAg-alloy-nanoprobe. Absorbance ratio of AuAg-alloy-nanoprobes (14 ρM) functionalized with the 1 OD/2.8 ml AuAgNPs ratio (**A**) and 1 OD/2 ml AuAgNPs ratio (**B**) alone - Blank; in the presence of a complementary target (23.3 ρmol) – MycoPOS; and in the presence of a non-complementary target (23.3 ρmol) – MycoNEG; in a 10 mM phosphate buffer pH 7 and a NaCl final concentration of 2.5 M (A). Orange bars represent non-aggregated nanoprobes and grey bars represent aggregation of the nanoprobes.

Discrimination between MycoPOS and MycoNEG is achieved, being more evident (higher Abs ratio) using the AuAg-alloy-nanoprobe synthesized using a 1 OD/2.8 ml AuAgNPs ratio (Figure 14). This can be explained with the load of ssDNA on the surface of the nanoparticle. The higher surface density of oligonucleotides functionalization for the nanoprobe synthesized with the 1 OD/2.8 ml AuAgNPs allows the hybridization of more complementary DNA molecules per AuAg-alloy-nanoprobe, thus conferring higher stability to a given ionic strength [35].

Further testing continued with the nanoprobe synthesized with the 1 OD/2.8 ml AuAgNPs ratio.

3.3.2 Utilization of AuAg nanoprobes in the detection of synthetic oligonucleotides

Due to the low yield of functionalization, DNA detection was carried out with a smaller AuAg-alloy-nanoprobe concentration (5 ρM) than used before. Hybridization assays were carried out as described in section 2.5.7. All assays were carried out in triplicate.

Complementary DNA detection was carried out using a synthetic complementary DNA sequence (herein designated as MycoPOS) or a non-complementary DNA sequence (herein designated as MycoNEG). As reference (blank), an assay where the DNA volume is replaced by buffer solution was carried out.

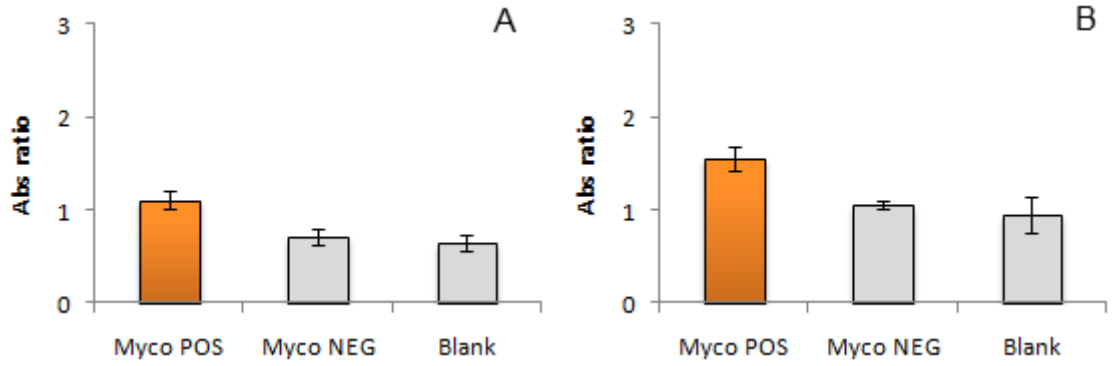

Figure 15: Detection of specific nucleic acids sequence with AuAg-alloy-nanoprobe. Absorbance ratio from visible spectra of AuAg-alloy-nanoprobes (5 ρM) alone - Blank; in the presence of a complementary target (23.3 ρmol) – MycoPOS; and in the presence of a non-complementary target (23.3 ρmol) – MycoNEG; in a 10 mM phosphate buffer pH 7 (A) or pH 8 (B) and a NaCl final concentration of 2 M. Orange bars represent non-aggregated nanoprobes and grey bars represent aggregation of the nanoprobes.

For a final DNA concentration of 23.3 ρmol and 2 M NaCl, although it is possible to observe discrimination between MycoPOS and MycoNEG, the Abs ratio is very close to 1 (Figure 15), consequence of the low absorbance values - Figure 16, meaning that discrimination is low between aggregated and non-aggregated samples.

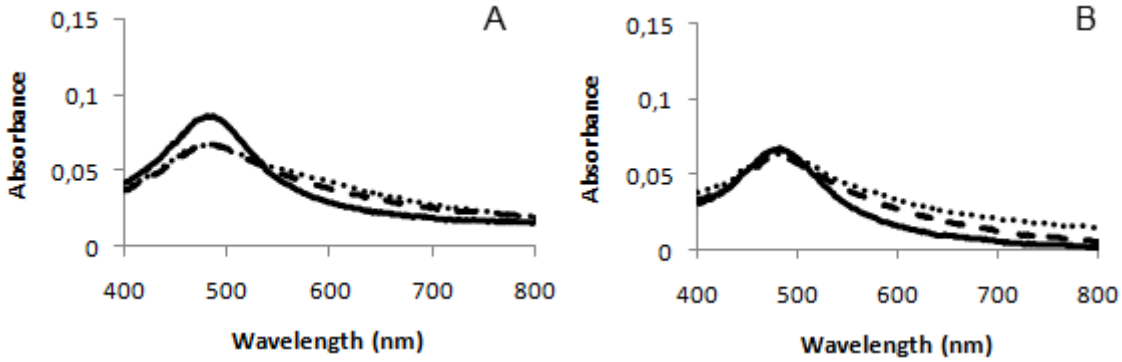

Figure 16: Detection of specific nucleic acids sequence with AuAg-alloy-nanoprobe. Visible spectra of AuAg-alloy-nanoprobes (5 ρM) alone – Blank (**––**); in the presence of a complementary target (23.3 ρmol) – MycoPOS (**—**); and in the presence of a non-complementary target (23.3 ρmol) – MycoNEG (**⋯**); in a 10 mM phosphate buffer pH 7 (A) or 8 (B) and a NaCl final concentration of 2 M.

This lead to the modification of the functionalization protocol (see section 3.2.2.2.) which allowed an increment in the procedure yield, thus a higher concentration (14 ρM) of AuAg-alloy-nanoprobe could be used.

The AuAg-alloy-nanoprobes efficiency in DNA detection was compared to that of an Au-nanoprobe (see annex 6.1 Figure 25 for Au-nanoprobe characterization). Comparing the Abs ratios (Figure 17), it is possible to observe that the AuAg-alloy-nanoprobes have comparable efficiency to the verified with their gold counterparts.

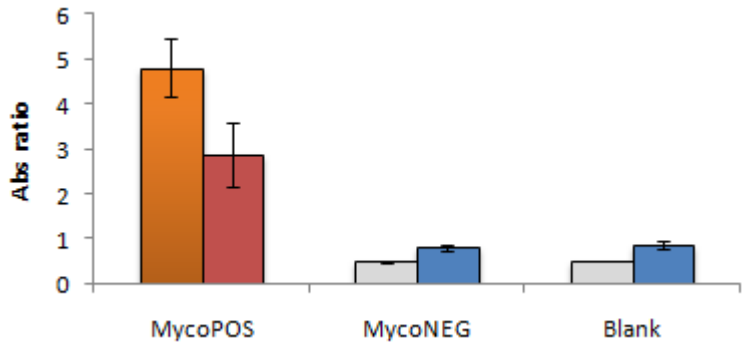

Figure 17: Detection of specific nucleic acids sequence with AuAg-alloy-nanoprobe and Au-nanoprobes. Absorbance ratio from visible spectra of AuAg-alloy-nanoprobes (14 ρM) and Au-nanoprobes (2.5 nM) alone - Blank; in the presence of a complementary target (23.3 ρmol) – MycoPOS; and in the presence of a non-complementary target (23.3 ρmol) – MycoNEG; in a 10 mM phosphate buffer pH 7 and a $MgCl_2$ final concentration of 0.02 M. Orange bars represent non-aggregated nanoprobes and grey bars represent aggregation of the nanoprobes (AuAg-alloy-nanoprobes). Red bars represent non-aggregated nanoprobes and blue bars represent aggregation of the nanoprobes (Au-nanoprobes).

3.3.2.1. AuAg-alloy-nanoprobes sensitivity

The AuAg-alloy-nanoprobes were able to detect as little as 70 fmol of a synthetic oligonucleotide (Figure 18). For this amount of target the Au-nanoprobe was unable to detect the presence of complementary DNA. However, sensitivity comparison between the two types of nanoprobes is not possible, as they have different nanoparticle sizes, different constitution, different surface functionalized oligonucleotides densities, factors that influence greatly the detection sensitivity.

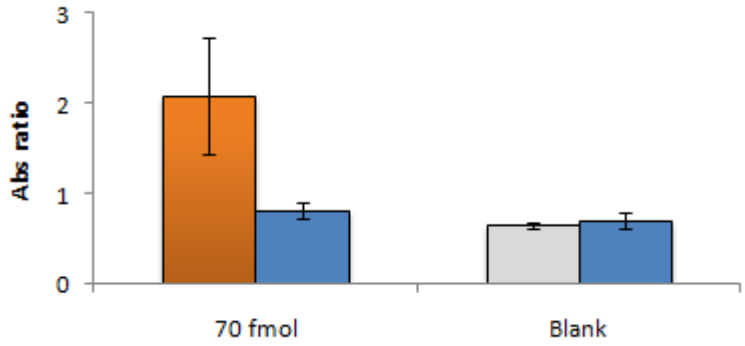

Figure 18: Detection of specific nucleic acids sequence with AuAg-alloy-nanoprobes and Au-nanoprobes. Absorbance ratio from visible spectra of AuAg-alloy-nanoprobes (14 ρM) and Au-nanoprobes (2.5 nM) in a 10 mM phosphate buffer pH 7, in the presence of 70 fmol of MycoPOS, a NaCl final concentration of 2.5 M (AuAg-alloy-nanoprobes) and a $MgCl_2$ final concentration of 0.02 M (Au-nanoprobe). Orange bars represent non-aggregated nanoprobes and grey bars represent aggregation of the nanoprobes. Red bars represent non-aggregated nanoprobes and blue bars represent aggregation of the nanoprobes (Au-nanoprobes).

3.3.3. Utilization of AuAg nanoprobes in detection of biological samples

To test the AuAg-alloy-nanoprobes robustness, following their initial characterization, they were used for detection of *M. tuberculosis* sequences in PCR amplified fragments derived from clinical samples (Figure 19A) and from plasmid DNA (Figure 19B).

Using the AuAg-alloy-nanoprobes, the discrimination between positive and negative samples was possible using as little as 5 ng/µL of DNA, which is more than the amount detected with the Au-nanoprobe system (Figure 19A).

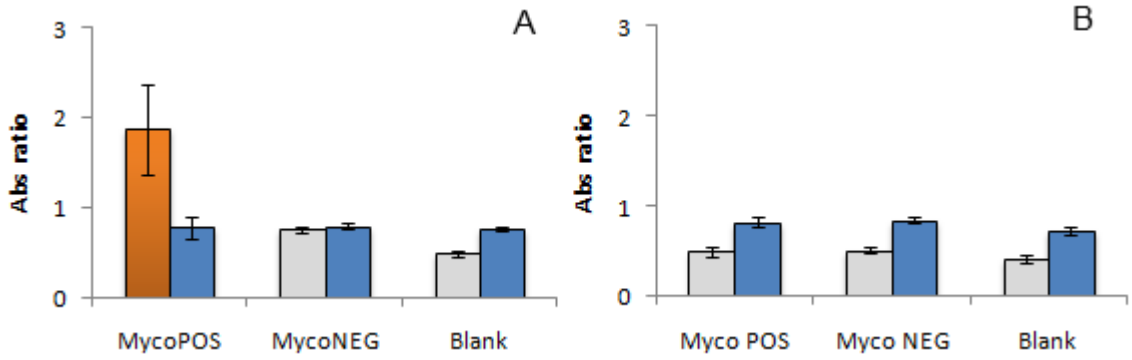

Figure 19: Detection of specific nucleic acids sequence with AuAg-alloy-nanoprobes and Au-nanoprobes. A. PCR product: Absorbance ratio from visible spectra of AuAg-alloy-nanoprobes (14 ρM) and Au-nanoprobes (2.5 nM) alone - Blank; in the presence of a complementary target (5 ng/µl of DNA in the form of PCR product) – MycoPOS; and in the presence of a non-complementary target (5 ng/µl of DNA in the form of PCR product) – MycoNEG; in a 10 mM phosphate buffer pH 7 and a $MgCl_2$ final concentration of 0.014 M (AuAg-alloy-nanoprobes) and 0.02 M (Au-nanoprobe). **B. Plasmid DNA:** Absorbance ratio from visible spectra of AuAg-alloy-nanoprobes (14 ρM) and Au-nanoprobes (2.5 nM) alone - Blank; in the presence of a complementary target (50 µg/µl of plasmid DNA) – MycoPOS; and in the presence of a non-complementary target (50 µg/µl of plasmid DNA) – MycoNEG; in a 10 mM phosphate buffer pH 7 and a $MgCl_2$ final concentration of 0.014 M (AuAg-alloy-nanoprobes) and 0.02 M (Au-nanoprobe). Orange bars represent non-aggregated nanoprobes and grey bars represent aggregation of the nanoprobes. Red bars represent non-aggregated nanoprobes and blue bars represent aggregation of the nanoprobes (Au-nanoprobes).

For these assays, AuAg-alloy-nanoprobes aggregation was induced using $MgCl_2$. The presence of a larger DNA fragment (the synthetic oligonucleotide used previously is only 36 bp in length, the PCR product has 384 bp in length) conferred stability, and a concentration up to 3 M of NaCl did not induce nanoprobe aggregation. This observation can be explained by both the electrostatic interaction between the DNA phosphate groups and the nanoparticles conferring stability to higher ionic strengths and by the steric hindrance against aggregation conferred by the target molecule [35].

The AuAg-alloy-nanoprobes detection of specific DNA in the form of plasmid DNA was also studied. After being able to detect DNA fragments of approximately 400 bp, this study had the objective of evaluate their efficiency in the detection of 10 fold longer DNA molecule.

Here, the discrimination between positive and negative samples was not possible with both nanoprobes tested (Figure 19B), even though up to 50 µg/ml of DNA was used. One can

hypothesize that for larger DNA sequences double strand renaturing is more favorable than hybridization of the nanoprobe to the target sequence.

4. Conclusion

The present work describes the modification of the citrate reduction method for the synthesis of gold-silver alloy nanoparticles and their functionalization with thiol-ssDNA. The synthesized AuAgNPs and AuAg-alloy-nanoprobes were chemical and spectroscopically characterized.

To our knowledge, this is the first report of functionalization of alloy gold-silver nanoparticles with thiol-ssDNA and their application in specific DNA detection. With these NPs one can take advantage of both the thiol affinity exhibited by gold and of the enhancement of the Surface Plasmon Resonance extinction coefficient conferred by silver.

By modifying the citrate reduction method for AuAgNPs synthesis, it was possible to obtain nanoparticles suitable for functionalization with thiol-ssDNA. The fact that the simple citrate reduction method is used instead of a more elaborated synthetic scheme, is an advantage when compared, e.g., to the complex synthesis for AuAg-coreshell-NPs for biomolecule detection [54,55,56].

The synthesized AuAg-alloy-nanoprobes were applied for specific sequence DNA detection via an adapted non-cross-linking method [35]. The AuAg-alloy-nanoprobes were capable to detect down to 70 fmol of a synthetic oligonucleotide and 5 ng/µL of a PCR amplified DNA. However, they were unable to detected specific sequences in more complex DNA samples, such as plasmid DNA, showing that the system still needs further optimization. A comparison between the sensitivity and efficiency of DNA detection with the described nanoprobes and their gold-only counterparts proved more difficult than expected. Despite of the standardization of the assays conditions, the fact that both types of nanoprobes differ in nanoparticle size and in surface density of the oligonucleotides used for functionalization, among other factors, did not allow a rigorous comparison between results obtained with both types of nanoprobes. Nevertheless, the use of AuAg-alloy-nanoprobes in DNA detection showed to have gold-like efficiency.

The results attained with this work, present a new class of DNA/nanoparticle hybrid materials and assemblies. However, further characterization is needed, namely:

- To study the influence of the sodium citrate concentration used in the NPs synthesis on their final size and composition,
- To assess the effect of the solution's ionic strength (promoted by other than the salts here tested) on the AuAgNPs SPR peak profile,
- To evaluate the use of thiol-ssDNA of different sequence length and their influence in the functionalization procedure,
- To test different spacers (e.g. amine) in the AuAgNPs functionalization,
- To investigate the possibility of functionalization with biomolecules other than nucleic acids (e.g. proteins).

AuAg-alloy-nanoprobes can in principle be used in a plethora of other methods and applications for nanodiagnostics, which following already described strategies for AuNPs [10] may give rise to new methodologies for biodetection.

As discussed, controlling the nanoparticles size, composition and nanostructure it is possible to create a unique absorbance signature. Thus, the synthesis of AuAgNPs with gold molar fractions different than the used in this work, the bimetallic NPs synthesis using different metal combinations (e.g., Cu, Pt) and the already well-established Au-nanoprobe system, all combined, can make way for the creation of new multiplex methods for specific biodetection.

5. References

[1] Niemeyer, C.M.; Mirkin C.A. (2004) Nanobiotechnology – Concepts, applications and perspectives. Wiley-CH Verlag GmbH & Co. KGaA. Weinheim, Germany.

[2] Wabuyele, M.B., Culha, M., Griffin, G.D., Viallet, P.M., and Vo-Dinh, T. (2005) Near-field scanning optical microscopy for bioanalysis at the nanometer resolution. Protein Nanotechnology. Ed. Humana Press. New Jersey, USA.

[3] Vo-Dinh, T. (2007) Nanotechnology in Biology and Medicine – Methods, Devices, and Applications. CRC Press Taylor & Francis Group. Florida, USA.

[4] Vo-Dinh, T.; Alarie, J.P.; Cullum, B.; Griffin, G.D. Antibody-based nanoprobe for measurements in a single cell, *Nat. Biotechnol.* **2000**, 18, 764-767.

[5] Kasili, P.M.; Song, J.M.; Vo-Dinh, T. Optical sensor for the detection of caspase-9 activity in a single cell. *J. Am. Chem. Soc.* **2004**, 126, 2799-2806.

[6] Kricka, L.J.; Fortina, P. Analytical Ancestry: “Firsts” in Fluorescent Labeling of Nucleosides, Nucleotides, and Nucleic Acids. *Clin. Chem*. **2009**, 55, 670-683.

[7] de Silva, A.P.; Gunaratne, H.Q.N.; Gunnlaugsson, T.; Huxley, A.J.M.; McCoy, C.P.; Rademacher, J.T.; Rice, T.E. Signaling Recognition Events with Fluorescent Sensors and Switches. *Chem. Rev.* **1997**, 97, 1515-1566.

[8] Rosi, N. L.; Mirkin, C. A. Nanostructures in Biodiagnostics. *Chem. Rev.* **2005**, 105, 1547–1562.

[9] Wang, H.; Yang, R.; Yang, L.; Tan, W. Nucleic Acid Conjugated Nanomaterials for Enhanced Molecular Recognition. *ACSNano* **2009**, 3, 2451-2460.

[10] Baptista, P.; Pereira, E.; Eaton, P.; Doria, G.; Miranda, A.; Gomes, I.; Quaresma, P.; Franco, R. Gold nanoparticles for the development of clinical diagnosis methods. *Anal Bioanal Chem.* **2008**, 391, 943–950.

[11] Mirkin, C.A.; Letsinger, R.L.; Mucic, R.C.; Storhoff, J.J. A DNA-based method for rationally assembling nanoparticles into macroscopic materials. *Nature*. **1996**, 382, 607-609.

[12] Ghosh, S. K.; Pal, T. Interparticle Coupling Effect on the Surface Plasmon Resonance of Gold Nanoparticles: From Theory to Applications. *Chem. Rev.* **2007**, 107, 4797–4862.

[13] Lee, P.C.; Meisel, D. Adsorption and surface-enhanced Raman of dyes on silver and gold sols. *J. Phys. Chem.* **1982**, 86, 3391–3395.

[14] Liu, G.L.; Rodriguez, V.B.; Lee, L.P. Time-Resolved Optical Sensing of Oligonucleotide Hybridization via Au Colloidal Nanoparticles. *J. Nanosci. Nanotechnol.* **2005**, 5, 1933-1937.

[15] Storhoff, J.J.; Elghanian, R.; Mirkin, C.A.; Letsinger, R.L. Sequence-Dependent Stability of DNA-Modified Gold Nanoparticles. *Langmuir.* **2002**, 18, 6666-6670.

[16] Storhoff, J.J.; Lazarides, A.A.; Mucic, R.C.; Mirkin, C.A.; Letsinger, R.L.; Schatz, G.C. What Controls the Optical Properties of DNA-Linked Gold Nanoparticle Assemblies? *J. Am.Chem.Soc.* **2000**, 122, 4640-4650.

[17] Taton, T.A.; Mirkin, C.A.; Letsinger, R.L. Scanometric DNA array detection with nanoparticle probes. *Science*. **2000**, 289. 1757-1760.

[18] Wang, Z.; Levy, R.; Fernig, D.G.; Brust, M. Kinase-Catalyzed Modification of Gold Nanoparticles: A New Approach to Colorimetric Kinase Activity Screening. *J.Am.Chem.Soc.* **2006**, 128, 2214-2215.

[19] Yu, C.X.; Irudayaraj, J. Multiplex Biosensor Using Gold Nanorods. *Anal. Chem.* **2007**, 79, 572-579.

[20] Eustis, S.; El-Sayed, M.A. Why gold nanoparticles are more precious than pretty gold: Noble metal surface plasmon resonance and its enhancement of the radiative and nonradiative properties of nanocrystals of different shapes. *Chem. Soc. Rev*. **2006**, 35, 209-217.

[21] Tabor, C.; Murali, R.; Mahmoud, M.; El-Sayed, M.A. On the Use of Plasmonic Nanoparticle Pairs As a Plasmon Ruler: The Dependence of the Near-Field Dipole Plasmon Coupling on Nanoparticle Size and Shape. *J.Phys.Chem.A.* **2009**, 113, 1946-1953.

[22] Mulvaney, P. Surface plasmon spectroscopy of nanosized metal particles. *Langmuir.* **1996**, 12, 788-800.

[23] Evanoff Jr., D.D.; Chumanov, G. Synthesis and Optical Properties of Silver Nanoparticles and Arrays. *ChemPhysChem.* **2005**, 6, 1221-1231.

[24] Mallin, M.P.; Murphy, C.J. Solution Synthesis of Sub-10 nm Au-Ag Alloy Nanoparticles. *Nano Letters*. **2002**, 2(11), 1235-1237.

[25] Kimling, J.; Maier, M.; Okenve, B.; Kotaidis, V.; Ballot, H.; Plech, A. Turkevich Method for Gold Nanoparticle Synthesis Revisited. *J. Phys. Chem. B.* **2006**, 110, 15700-15707.

[26] Turkevich, J.; Hillier, J.; Stevenson, P. C. Nucleation and Growth Process in the Synthesis of Colloidal Gold. *Discussions Faraday Soc.* **1951**, 11, 55-75.

[27] Marin, M.L.; McGilvray, K.L.; Scaiano, J.C. Photochemical strategies for the synthesis of gold nanoparticles from Au(III) and Au(I) using photoinduced free radical generation. *J. Am. Chem. Soc.* **2008**, 130(49), 16572-16584.

[28] Das, S.K.; Das, A.R.; Guha, A.K. Gold nanoparticles: microbial synthesis and application in water hygiene management. *Langmuir*. **2009**, 25(14), 8192-8199.

[29] Love, J.C.; Estroff, L.A.; Kribel, J.K.; Nuzzo, R.G.; Whitesides, G.M. Self-Assembled Monolayers of Thiolates on Metals as a Form of Nanotechnology. *Chem.Rev.* **2005**, 105, 1103-1169.

[30] Liu, X.; Dai, Q.; Austin, L.; Coutts, J.; Knowles, G.; Zou, J.; Chen, H.; Huo, Q. A one-step homogeneous immunoassay for cancer biomarker detection using gold nanoparticle probes coupled with dynamic light scattering. *J. Am. Chem. Soc*. **2008**, 130, 2780-2782.

[31] Huang, X.; Jain, P.K.; El-Sayed, I.H.; El-Sayed, M.A. Plasmonic photothermal therapy (PPTT) using gold nanoparticles. *Lasers Med. Sci.* **2008**, 23, 217-228.

[32] Han, G.; Ghosh, P.; Rotello, V.M. Functionalized gold nanoparticles for drug delivery. *Nanomedicine*. **2007**, 2, 113-123.

[33] Storhoff, J.J.; Lucas, A.D.; Garimella, V.; Bao, Y.P.; Muller, U.R. Homogeneous detection of unamplified genomic DNA sequences based on colorimetric scatter of gold nanoparticle probes. *Nat Biotechnol*. **2004**, 22, 883–887.

[34] Zhao, W.; Brook, M. A.; Li, Y. F. Design of Gold Nanoparticle-Based Colorimetric Biosensing Assays. *ChemBioChem* **2008**, 9, 2363–2371.

[35] Baptista, P.; Doria, G.; Henriques, D.; Pereira, E.; Franco, R. Colorimetric detection of eukaryotic gene expression with DNA-derivatized gold nanoparticles. *Journal of Biotechnology.* **2005**, 119, 111-117.

[36] Baptista, P.V.; Koziol-Montewka, M.; Paluch-Oles, J.; Doria, G.; Franco, R. Gold-Nanoparticle-Probe–Based Assay for Rapid and Direct Detection of *Mycobacterium tuberculosis* DNA in Clinical Samples. *Clin. Chem.* **2006**, 52, 1433-1434.

[37] Doria, G.; Franco, R.; Baptista, P. Nanodiagnostics: fast colorimetric method for single nucleotide polymorphism/mutation detection. *IET Nanobiotechnol.* **2007**, 1, 53-57.

[38] Huber, M.; Wei, T.; Müller, U.; Lefebvre, P.A.; Marla, S.S.; Bao, Y.P. Gold nanoparticle probe-based gene expression analysis with unamplified total human RNA. *Nucleic Acids Research* **2004**, 32, e137.

[39] Kreibig, U.; Vollmer, M. *Optical Properties of Metal Clusters*. **1995**, Springer Series in Materials Science 25. Springer-Verlag, 50, New York, USA.

[40] Evanoff Jr., D.D.; Chumanov, G. Size-Controlled Synthesis of Nanoparticles. 2. Measurement of Extinction, Scattering and Absorption Cross Sections. *J.Phys.Chem.B* **2004**, 108, 13957-13962.

[41] Thompson, D.G.; Enright, A.; Faulds, K.; Smith, W.E.; Graham, D. Ultrasensitive DNA Detection Using Oligonucleotide-Silver Nanoparticle Conjugates. *Anal.Chem.* **2008**, 80, 2805-2810.

[42] Lee, J.; Lytton-Jean, A.K.R.; Hurst, S.J.; Mirkin, C.A. Silver Nanoparticle-Oligonucleotide Conjugates Based on DNA with Triple Cyclic Disulfide Moieties. *Nano Lett.* **2007**, 7, 2112-2115

[43] Tokareva, I.; Hutter, E. Hybridization of Oligonucleotide-Modified Silver and Gold Nanoparticles in Aqueous Dispersions and on Gold Films. *J.Am.Chem.Soc.* **2004**, 126, 15784-15789.

[44] Vidal Jr., B.C.; Deivaraj, T.C.; Yang, J.; Too, H.; Chow, G.; Gan, L.; Lee, J.Y. Stability and hybridization-driven aggregation of silver nanoparticle-oligonucleotide conjugates. *New J. Chem.* **2005**, 29, 812-816.

[45] Lang, H.; Maldonado, S.; Stevenson, K.J.; Chandler, B.D. Synthesis and Characterization of Dendrimer Templated Supported Bimetallic Pt-Au Nanoparticles. *J. Am. Chem. Soc.* 2004, 126, 12949–12956.

[46] Lu, P. Teranishi, T.; Asakura, K.; Miyake, M.; Toshima, N. Polymer-Protected Ni/Pd Bimetallic Nano-Clusters; Preparation, Characterization and Catalysis for Hydrogenation of Nitrobenzene. *J. Phys. Chem. B*. 1999, 103, 9673–9682.

[47] Harada, M.; Asakura, K.; Toshima, N. Catalytic Activity and Structural Analysis of Polymer-Protected Au/Pd Bimetallic Clusters Prepared by the Successive Reduction of HauC14 and PdClz. *J.Phys.Chem.* **1993**, 97, 5103-5114.

[48] Link, S.; Wang, Z.L.; El-Sayed, M.A. Alloy Formation of Gold-Silver Nanoparticles and the Dependence of the Plasmon Absorption on Their Composition. *J. Phys. Chem. B.* **1999**, 103, 3529-3533.

[49] Sun, S.; Murray, C.B.; Weller, D.; Folks, L.; Moser, A. Monodisperse FePt Nanoparticles and Ferromagnetic FePt Nanocrystal Superlattices. *Science*. **2000**, 287, 1989-1992.

[50] Salem, A.K.; Searson, P.C.; Leong, K.W. Multifunctional nanorods for gene delivery. *Nature Materials*. **2003**, 2, 668-671.

[51] Pullen, A.; Zeltner, S.; Olk, R.; Hoyer, E.; Abboud, K.A.; Reynolds, J.R. Electrically Conducting Materials Based On μ-Tetrathiooxalato-Bridged Bimetallic Ni(II) Anionic Complexes. *Inorg. Chem.* 1997, 36, 4163–4171.

[52] Douglas, F.; Yañez, R.; Ros, J.; Marín, S.; de la Escosura-Muñiz, A.; Alegret, S.; Merkoçi, A. Silver, gold and the corresponding core shell nanoparticles: synthesis and characterization. *J.Nanopart.Res.* **2008**, 10, 97-106.

[53] Wilcoxon, J. Optical Absorption Properties of Dispersed Gold and Silver Alloy Nanoparticles. *J. Phys. Chem. B.* **2009**, 113 (9), 2647–2656.

[54] Cao, Y.; Jin, R.; Mirkin, C.A. DNA-Modified Core-Shell Ag/Au Nanoparticles. *J.Am.Chem.Soc.* **2001**, 123, 7961-7962.

[55] Cao, Y.; Jin, R.; Thaxton, C.S.; Mirkin, C.A. A two-color-change, nanoparticle-based method for DNA detection. *Talanta*. **2005**, 67, 449-455

[56] Lim, D.; Kim, I.; Nam, J. DNA-embedded Au/Ag core-shell nanoparticles. *ChemComm*. **2008**, 5312-5314.

[57] Mulvaney, P.; Giersig, M.; Henglein, A. Electrochemistry of multilayer colloids: preparation and absorption spectrum of gold-coated silver particles. *J.Phys.Chem.* **1993**, 97, 7061-7064.

[58] Lee, P.C.; Meisel, D. Adsorption and surface-enhanced Raman of dyes on silver and gold sols. *J.Phys.Chem.* **1982**, 86, 3391-3395.

[59] Wang, A.; Chang, C.; Mou, C. Evolution of Catalytic Activity of Au-Ag Bimetallic Nanoparticles on Mesoporous Support for CO Oxidation. *J.Phys.Chem. B.* **2005**, 109, 18860-18867.

[60] Smith, N.H.; Hewinson, R.G.; Kremer, K.; Brosch, R.; Gordon, S.V. Myths and misconceptions: the origin and evolution of *Mycobacterium tuberculosis*. *Nature Reviews Microbiology* **2009**, 7, 537-544.

[61] Kenneth Todar (2009). *Todar's Online Textbook of Bacteriology* [online]. Available: http://www.textbookofbacteriology.net/tuberculosis.html [accessed 14 September 2009].

[62] Soini, H.; Musser, J.M. Molecular diagnosis of mycobacteria [Review]. *Clin. Chem.* **2001**, 47, 809–814

[63] Hurst, S.J.; Lytton-Jean, A.K.R.; Mirkin, C.A. Maximizing DNA Loading on a Range of Gold Nanoparticle Sizes. *Anal Chem.* **2006**, 78 (24), 8313–8318.

[64] Elghanian, R.; Storhoff, J.J.; Mucic, R.C.; Letsinger, R.L.; Mirkin, C.A. Selective Colorimetric Detection of Polynucleotides Based on the Distance-Dependent Optical Properties of Gold Nanoparticles. *Science.* **1997**, 277, 1078-1080.

[65] Papavassiliou, G.C. Surface plasmons in small Au-Ag alloy particles. *J.Phys.F: Met. Phys.* **1976**, 6, L103-L105.

[66] Mallin, M.P.; Murphy, C.J. Solution-Phase Synthesis of Sub-10 nm Au-Ag Alloy Nanoparticles. *Nanoletters*. **2002**, 2, 1235-1237.

[67] Liu, X.; Atwater, M.; Wang, J.; Huo, Q. Extinction coefficient of gold nanoparticles with different sizes and different capping ligands. *Colloids and Surfaces B: Biointerfaces*. **2007**, 58, 3-7.

[68] Weisbecker, C.S.; Mettir, M.V.; Whitesides, G.M. Molecular Self-Assembly of Aliphatic Thiols on Gold Colloids. *Langmuir.* **1996,** 12, 3763-3772.

[69] Burns, C.; Spendel, W.U.; Puckett, S.S.; Pacey, G.E. Solution ionic strength effect on gold nanoparticle solution color transition. *Talanta*. **2006**, 69, 873-876.

[70] Hunter, R.J. Foundations of Colloid Science, vol.1, *Clarendon Press, Oxford*, **1993**, pp. 329-341, 415-418.

[71] Demers, L.M; Mirkin, C.A.; Mucic, R.C.; Reynolds, R.A.; Letsinger, R.L.; Elghanian, R.; Viswanadham, G. A Fluorescence-Based Method for Determining the Surface Coverage and Hybridization Efficiency of Thiol-Capped Oligonucleotides Bound to Gold Thin Films and Nanoparticles. *Anal. Chem.* **2000**, 72, 5535-5541.

[72] Hill, H.D.; Millstone, J.E.; Banholzer, M.J.; Mirkin, C.A. The Role Radius of Curvature Plays in Thiolated Oligonucleotide Loading on Gold Nanoparticles. *ACSNano*. **2009**, 3, 418-424.

[73] Sigel, A.; Sigel H. (1996) Metal Ions in Biological Systems: Interactions of Metal Ions with Nucleotides, Nucleic Acids and Their Constituents v.32. New York, M. Dekker.

[74] Eaton, P.; Doria, G.; Pereira, E.; Baptista, P.V; Franco, R. Imaging Gold Nanoparticles for DNA Sequence Recognition in Biomedical Applications. *IEEE Transactions on nanobioscience.* **2007**, 6, 282-288.

[75] Vo-Dinh, T. Surface-enhanced Raman spectroscopy using metallic nanostructures. *Trends Anal.Chem.* **1998**, 17, 557-582.

[76] Gupta, S.; Huda, S.; Kilpatrick, P.K.; Velev, O.D. Characterization and optimization of gold nanoparticle- based silver-enhanced immunoassays. *Anal. Chem.* **2007**, 79, 3810-3820.

[77] Kelly, K.L.; Coronado, E.; Zhao, L.L.; Schatz, G.C. The Optical Properties of Metal Nanoparticles: The Influence of Size, Shape, and Dielectric Environment. *J. Phys. Chem. B.* **2003**, 107, 668-677.

[78] Kittel, C. (1996) Introduction to Solid State Physics. New York, Willey.

[79] Fang, X. H.; Li, J. J.; Perlette, J.; Tan, W. H.; Wang, K. M. Peer Reviewed: Molecular Beacons: Novel Fluorescent Probes. *Anal. Chem.* **2000**, 72, 747A–753A.

[80] Josephson, L.; Perez, J. M.; Weissleder, R. Magnetic Nanosensors for the Detection of Oligonucleotide Sequences. *Angew. Chem., Int. Ed.* **2001**, 40, 3204–3206.

[81] Major, K.J.; De, C.; Obare, S.O. Recent Advances in the Synthesis of Plasmonic Bimetallic Nanoparticles. *Plasmonics*. **2009**, 4, 61-78.

6. Annex

6.1. UV-Visible spectra

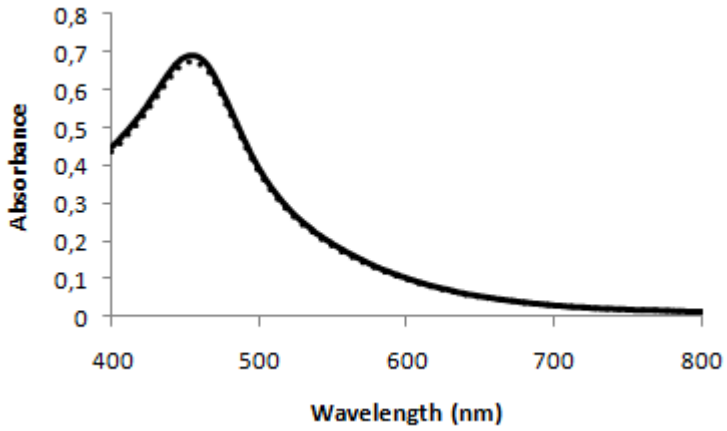

Figure 20: AuAgNPs stability against pH variation. Visible spectra of AuAgNPs obtained by Link, Wang and El-Sayed method in 10 mM phosphate buffer pH 7 (—) and in 10 mM phosphate buffer pH 8 (···) at room temperature.

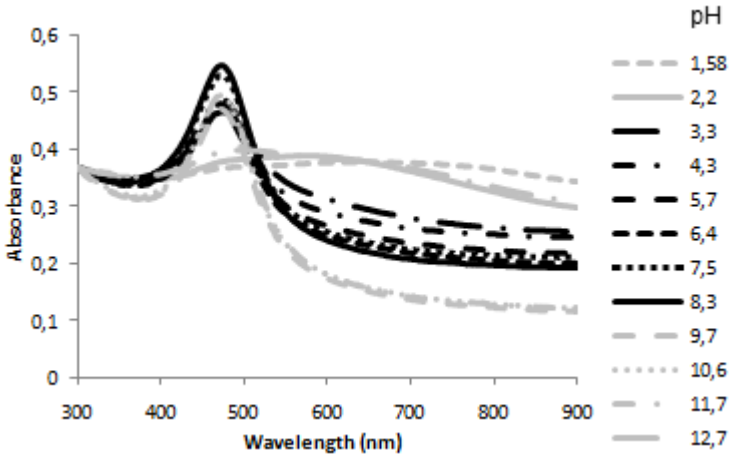

Figure 21: AuAgNps stability against pH-induced aggregation. Visible spectra of AuAgNPs obtained *Dias* method at different values of pH, at room temperature.

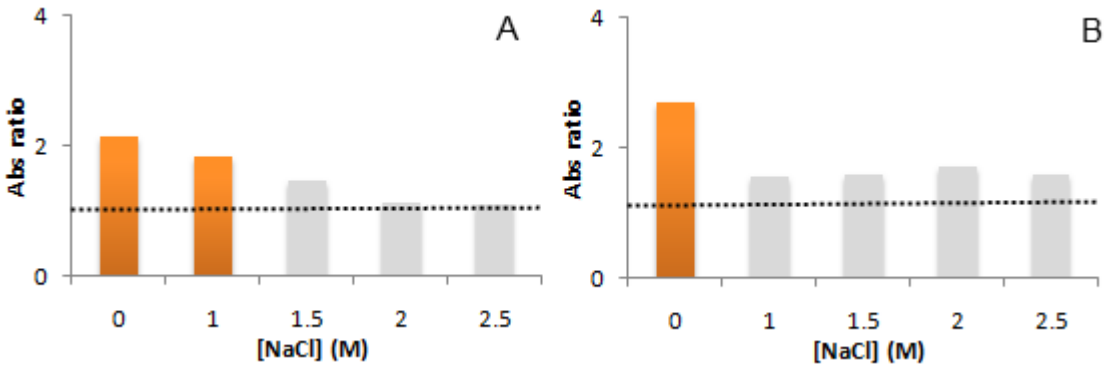

Figure 22: AuAg-alloy-nanoprobe stability against salt-induced aggregation. Visible spectra of AuAg-alloy-nanoprobes (5pM; 1 OD/2.8 ml AuAgNPs) in 10 mM phosphate buffer pH 7 (A), or pH 8 (B), at different salt (NaCl) concentrations. Orange bars represent non-aggregated nanoprobes and grey bars represent aggregation of the nanoprobes.

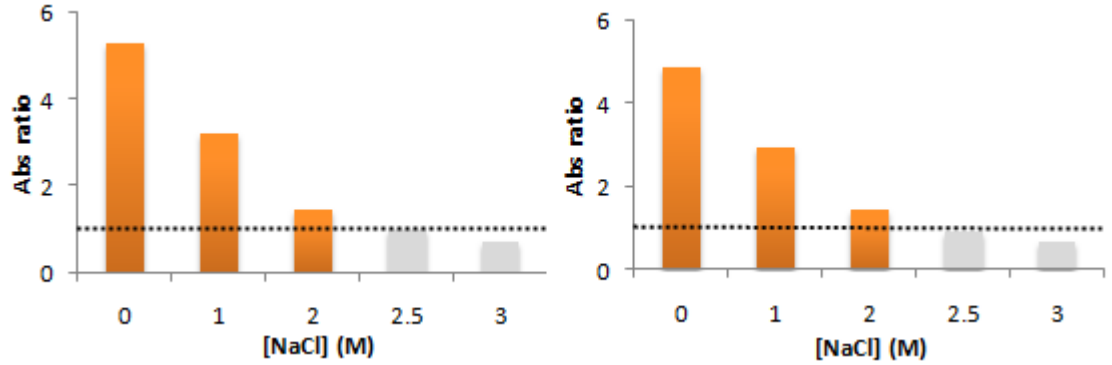

Figure 23: AuAg-alloy-nanoprobe stability against salt-induced aggregation. Visible spectra of AuAg-alloy-nanoprobes (14pM; 1 OD/2.8 ml AuAgNPs) in 10 mM phosphate buffer pH 7 (A), or pH 8 (B), at different salt (NaCl) concentrations. Orange bars represent non-aggregated nanoprobes and grey bars represent aggregation of the nanoprobes.

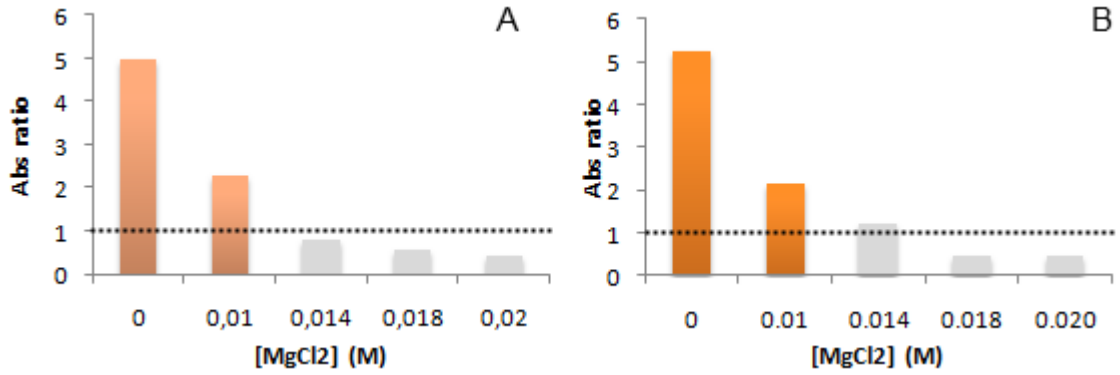

Figure 24: AuAg-alloy-nanoprobe stability against salt-induced aggregation. Visible spectra of AuAg-alloy-nanoprobes (14pM; ratio oligonucleotide/AuAgNPs: $6.2x10^4$) in 10 mM phosphate buffer pH 7 (A), or pH 8 (B), at different salt ($MgCl_2$) concentrations. Orange bars represent non-aggregated nanoprobes and grey bars represent aggregation of the nanoprobes.

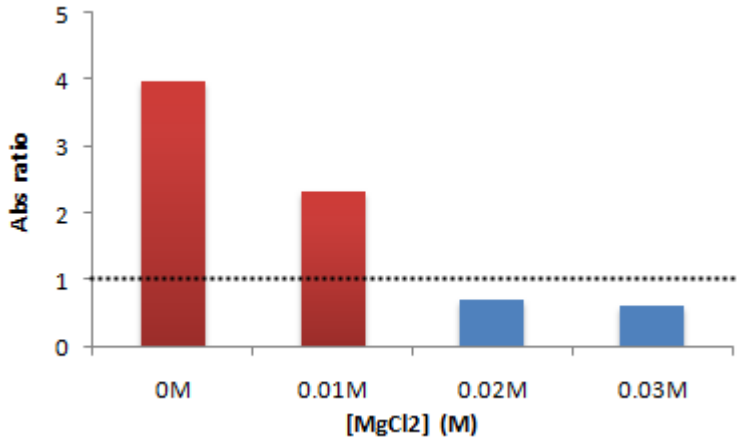

Figure 25: Au-nanoprobe stability against salt-induced aggregation. Visible spectra of Au-nanoprobes (0.25 nM;1 OD/2 ml AuNPs ratio) in 10 mM phosphate buffer pH 7 at different salt ($MgCl_2$) concentrations. Red bars represent non-aggregated nanoprobes and blue bars represent aggregation of the nanoprobes.

6.2. Calculation of the elemental composition

6.2.1. AuAgNPs – Link, Wang and El-Sayed method

Table 6: ICP characterization of the AuAgNPs.

Element	Concentration (g/l)
(Ag)	0.020
(Au)	0.013

[Au] (mol/l) = [Au] (g/l) / MM_{Au} (g/mol) = 0.013 / 196.97 = $1.02x10^{-4}$ mol/l

[Ag] (mol/l) = [Ag] (g/l) / MM_{Ag} (g/mol) = 0.020 / 107.87 = $1.21x10^{-4}$ mol/l

Elemental composition:

Au = [Au] (mol/l) / ([Au] (mol/l) + [Ag] (mol/l) = $1.02x10^{-4}$ / ($1.02x10^{-4}$ + $1.21x10^{-4}$)

= 0.46 => 46%

Ag = [Ag] (mol/l) / ([Au] (mol/l) + [Ag] (mol/l) = $1.21x10^{-4}$ / ($1.02x10^{-4}$ + $1.21x10^{-4}$)

= 0.54 => 54%

6.2.2. AuAgNPs – *Dias* method

Table 7: ICP characterization of the AuAgNPs.

Element	Concentration (g/l)
(Ag)	0.0046
(Au)	0.0082

[Au] (mol/l) = [Au] (g/l) / MM_{Au} (g/mol) = 0.0082 / 196.97 = $4.17x10^{-5}$ mol/l

[Ag] (mol/l) = [Ag] (g/l) / MM_{Ag} (g/mol) = 0.0046 / 107.87 = $4.28x10^{-5}$ mol/l

Elemental composition:

Au = [Au] (mol/l) / ([Au] (mol/l) + [Ag] (mol/l) = $4.17x10^{-5}$ / ($4.17x10^{-5}$ + $4.28x10^{-5}$)

= 0.49 => 49%

Ag = [Ag] (mol/l) / ([Au] (mol/l) + [Ag] (mol/l) = $4.28x10^{-5}$ / ($4.17x10^{-5}$ + $4.28x10^{-5}$)

= 0.51 => 51%

6.3. Calculation of molar extinction coefficients

6.3.1. AuAgNPs – Link, Wang and El-Sayed method

Compound/element	Molecular weight (g/mol)	Metal	Density (g/m^3)	Metal	[Metal] (mol/l)		
(HAuCl4)	393.87	Au	$1.93x10^7$	Au	$1.02x10^{-4}$	**NP radius (m)**	$1.25x10^{-8}$
(AgNO3)	169.87	Ag	$1.05x10^7$	Ag	$1.21x10^{-4}$	**NP volume (m^3)**	$8.14x10^{-24}$
(Au)	196.97						
(Ag)	107.87						

n_{Au} (mol) = $Volume_{total}$ (l) x [Au] (mol/l) = 0.25 X $1.02x10^{-4}$ = $2.55x10^{-5}$ mol

n_{Ag} (mol) = $Volume_{total}$ (l) x [Ag] (mol/l) = 0.25 X $1.21x10^{-4}$ = $2.83x10^{-5}$ mol

m_{Au} (g) = n_{Au} (mol) x MM_{Au} (g/mol) = $2.55x10^{-5}$ x 196.97 = $5.02x10^{-3}$ g

m_{Ag} (g) = n_{Ag} (mol) x MM_{Ag} (g/mol) = $2.83x10^{-5}$ x 107.87 = $3.06x10^{-3}$ g

Volume occupied by all NP:

$Volume_{Au} = m_{Au}$ (g) / d_{Au} (g/m^3) = $2.60x10^{-10}$ m^3

$Volume_{Ag} = m_{Ag}$ (g) / d_{Ag} (g/m^3) = $2.91x10^{-10}$ m^3

$Volume_{total} = Vol_{Au} + Vol_{Ag} = 2.60x10^{-10} + 2.91x10^{-10} = 5.51x10^{-10}$ m^3

Total of NPs = $Volume_{total}$ (m^3) /NP volume (m^3) = $5.51x10^{-10}$ / $8.14x10^{-24}$ = $6.73x10^{13}$

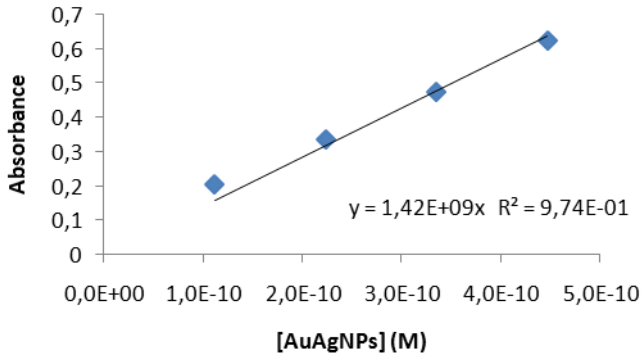

Figure 26: Calibration curve for molar extinction coefficient calculation.

$$\varepsilon = 1.42 \times 10^{9}\ M^{-1}\ cm^{-1}$$

6.3.2. AuAgNPs – *Dias* method

Compound/element	Molecular weight (g/mol)	Metal	Density (g/m^3)	Metal	[Metal] (mol/l)		
(HAuCl4)	393.87	Au	1.93×10^{7}	Au	4.17×10^{-5}	**NP radius (m)**	2.10×10^{-8}
(AgNO3)	169.87	Ag	1.05×10^{7}	Ag	4.28×10^{-5}	**NP volume (m^3)**	3.88×10^{-24}
(Au)	196.97						
(Ag)	107.87						

n_{Au} (mol) = $Volume_{total}$ (l) x [Au] (mol/l) = 0.25 X 1.02×10^{-4} = 1.04×10^{-5} mol

n_{Ag} (mol) = $Volume_{total}$ (l) x [Ag] (mol/l) = 0.25 X 1.13×10^{-4} = 1.07×10^{-5} mol

m_{Au} (g) = n_{Au} (mol) x MM_{Au} (g/mol) = 2.55×10^{-5} x 196.97 = 2.06×10^{-3} g

m_{Ag} (g) = n_{Ag} (mol) x MM_{Ag} (g/mol) = 2.83×10^{-5} x 107.87 = 1.16×10^{-3} g

Volume occupied by all NP:

$Volume_{Au} = m_{Au}$ (g) / d_{Au} (g/m^3) = 1.06×10^{-10} m^3

$Volume_{Ag} = m_{Ag}$ (g) / d_{Ag} (g/m^3) = 1.10×10^{-10} m^3

$Volume_{total} = Vol_{Au} + Vol_{Ag} = 1.06x10^{-10} + 1.10x10^{-10} = 2.16x10^{-10}\ m^3$

Total of NPs = $Volume_{total}$ (m^3) /NP volume (m^3) = $2.16x10^{-10} / 3.88x10^{-24} = 5.58x10^{12}$

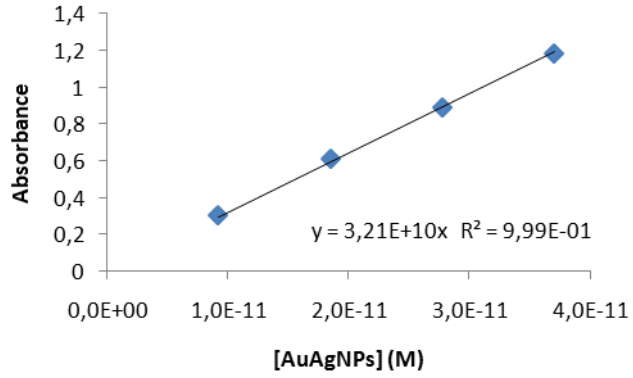

Figure 27: Calibration curve for molar extinction coefficient calculation.

$\varepsilon = 3.21x10^{10}\ M^{-1}\ cm^{-1}$